UNIVERSITÀ DEGLI STUDI DI PADOVA

Dipartimento di Fisica e Astronomia "Galileo Galilei"

Master Degree in Physics

Final Dissertation

Circuit complexity in the presence of a defect

Thesis supervisor

Prof. Alessandro Sfondrini

Thesis co-supervisor

Prof. Erik Tonni

Candidate

Francesco Gentile

Academic Year 2020/2021

Abstract

We study circuit complexity for the ground state of a harmonic chain with defect in 1+1 dimensions, choosing as a reference state, the ground state of the homogeneous chain. By employing the covariance matrix formalism, we compute numerically $\mathcal{C}_2$ complexity and extract its divergence pattern in the continuum limit. We find that, upon a suitable choice of the coordinates, $\mathcal{C}_2$ complexity displays a logarithmic divergence. Finally, we compare our results with the existing ones for the entanglement entropy of half chain and the holographic complexity in the presence of a defect.

Contents

1 Introduction

The concept of quantum circuit complexity has attracted considerable interest in quantum information since the beginning of the quantum computing era [1, 2]. In the simplest possible model for a quantum computer, we consider a collection of qubits $|q_i\rangle$, - the quantum analogue of classical bits - and a set of elementary gates U_I, - unitary operators typically acting on few qubits. Then, a quantum circuit can be regarded as a sequence of elementary gates implementing a unitary transformation $U = \Pi_{I=1}^{N} U_I$ on some unentangled state of the qubits, namely the reference state $|\psi_R\rangle = |q_1, \ldots, q_N\rangle$. The final state reached by the circuit is the target state:

$$|\psi_T\rangle = U\,|\psi_R\rangle\,. \tag{1.1}$$

A pictorial representation of a quantum circuit is given in figure 1.

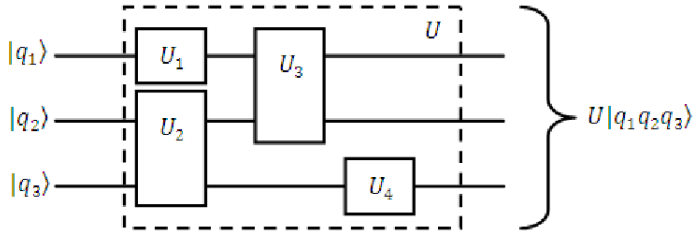

Figure 1: Pictorial representation of a quantum circuit.

In general, there is not a unique way to achieve a certain task with a quantum circuit and some circuits are more expensive than other in terms of the number of gates employed. One question naturally arises and regards the search for the optimal circuit to accomplish a certain task. This leads to define complexity as the minimal number of elementary gates required to implement the unitary transformation connecting the desired target and the reference state [1, 2].

This definition, besides its intuitive nature, is technically unfeasible and makes the estimate of complexity a rather difficult task. This is why Nielsen and collaborators introduced the geometric approach to complexity [3–5]. Their idea consisted in considering the space of all unitary transformations, which can be realized with a quantum circuit, and in equipping it with a geometric structure, allowing us to estimate the length of paths within such space. Complexity is then identified with the minimal length of the optimal path connecting the identity operator to the desired unitary transformation. The power of such approach resides in the fact that, if we are able to equip the space of unitaries with the structure of a Riemannian manifold, estimating complexity is related to the well known problem of finding geodesics.

It should be stressed that all the techniques developed by quantum information scientists are confined to the realm of quantum mechanics with a finite number of degrees of freedom. However, in more recent times quantum field theorists and high energy physicists have turned their eye onto the notion of complexity and have been putting increasing effort into understanding complexity in a quantum field theory framework. In order to bridge the gap between quantum information and quantum field theory, a lattice quantum field theory perspective has been adopted [6–16]. Considering a discrete version of free scalar and fermionic field theories, Nielsen's approach has been applied to these lattice theories and the behavior of complexity in their continuum limit has been studied. In order to make the problem more tractable, the attention has been restricted to Gaussian states, which are a well known class of states in quantum information literature [17–21]. Within this perspective, complexity has also been quantified for quantum circuits made by mixed states, which are characterized by density matrices [22–27]. Moreover, some attempts have been made to characterize complexity for weakly interacting quantum field theories using Nielsen's approach in a lattice framework [28]. We should finally mention that a purely quantum field theory definition of complexity is still lacking and that in the last few years a good amount of effort has been put in such direction [29–39]. At the moment, the lattice field theory approach still remains the best tool to estimate complexity in free and weakly interacting theories, whereas still very little is known about complexity in strongly interacting theories.

Besides being it an interesting problem in itself, the main motivation for a quantum field theory definition of complexity lies in the field of the (holographic) gauge/gravity correspondence between quantum (gauge) field theories and quantum gravity models from string theory. The main idea behind the holographic principle is that a theory of (quantum) gravity whose dynamics takes place in a certain volume V is equivalent to a non-gravitational theory living in the boundary ∂V [40,41]. Such principle was realized in the so called AdS/CFT correspondence [42–45], which consists in a duality between a gravitational theory living in the Anti de Sitter space (AdS) and conformal field theory (CFT) living on its boundary. It should be stressed that this is a strong/weak coupling duality, which basically means that the strong coupling regime on one side of the correspondence is a strongly coupled regime on the other side: therefore the dual CFT to a semiclassical theory of gravity, will be a strongly coupled one.

In the AdS/CFT framework, it is natural to introduce a dictionary connecting gravitational observables in the bulk to quantum field theory observables living in the boundary. It is exactly in the search of such dictionary that the relationship between quantum information and gravity soon became evident. One of the most important results is the formula for the holographic entanglement entropy [46–48] which relates the entanglement entropy in a CFT at

strong coupling to a classical gravitational observable. To be more precise, the entanglement entropy associated to the subregion A in the boundary is seen to be proportional to the area of the so called Ryu-Takayanagi surface γ_A, defined as the minimal area surface in the bulk such that it is homologous to the subregion A and it has the same boundary as A, i.e. $\partial\gamma_A = \partial A$:

$$S_A = \frac{Area(\gamma_A)}{4G_N}. \tag{1.2}$$

A pictorial representation of the prescription for the holographic entanglement entropy is given in figure 2.

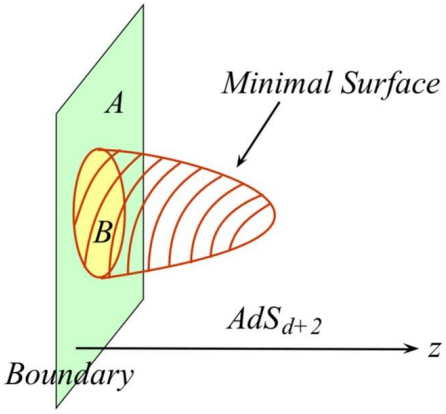

Figure 2: Pictorial representation of the prescription for the holographic entanglement entropy. Figure taken from [49].

Motivated by the success of the proposal for the holographic entanglement entropy [50, 51], many attempts were made in order to find the gravitational dual of other quantum information observables, among which there is certainly complexity [52–61]. At the moment two main proposals are being investigated: complexity equals volume ($\mathcal{CV}$) and complexity equals action ($\mathcal{CA}$). According to $\mathcal{CV}$ [52, 55], holographic complexity is proportional to the volume $\mathcal{V}$ of a maximal codimension-one bulk surface $\mathcal{B}$ that extends to the AdS boundary, and asymptotes to the time slice Σ on which the boundary state is defined:

$$C_V = \max_{\Sigma=\partial\mathcal{B}} \left[\frac{\mathcal{V}(\mathcal{B})}{G_N L} \right], \tag{1.3}$$

where L is some length scale associated with the bulk geometry, usually the AdS radius or the radius of the black hole. In the case of the eternal AdS black hole, the surface $\mathcal{B}$ is the Einstein-Rosen bridge (ERB) connecting the time slices t_L and t_R on the left and the right boundary. This can be seen in the left

panel of figure 3. The $\mathcal{CA}$ proposal instead states that holographic complexity is proportional to the gravitational action I_{WDW} evaluated on the Wheeler-De Witt (WDW) [58,59]:

$$\mathcal{C}_A = \frac{I_{WDW}}{\pi}. \tag{1.4}$$

The WDW patch is defined as the union of all spacelike surfaces anchored at the boundary time slice where the quantum state lives and can be regarded as the causal development of the surface $\mathcal{B}$ defined for the $\mathcal{CV}$ conjecture. In the left panel of figure 3, we can see the WDW patch in the eternal AdS black hole, anchored at the time slices t_L and t_R on the left and right boundary.

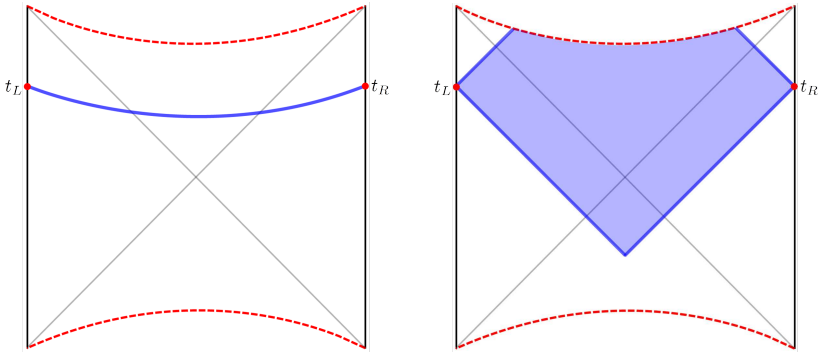

Figure 3: $\mathcal{B}$ surface and WDW patch in the eternal AdS black hole. Figure taken from [6].

In order to test those two conjectures, we need to calculate complexity in the framework of the dual CFT. However, as it has been previously stated, at the moment a precise definition of complexity in a pure quantum field theory framework lacks completely and there is no method to evaluate complexity in a strongly interacting CFT which is often of interest in holography. The best that can be done for complexity is to calculate it for the Gaussian states of the lattice version of a free quantum field theory. Then the divergence pattern of complexity in the continuum limit of lattice free theories can be compared to that of the gravitational observables for holographic complexity. We stress that this comparison is not the one that should be rigorously made in the framework of AdS/CFT correspondence, because holographic complexity is computed in a general relativity framework and therefore the dual quantum field theory complexity should be computed within the framework of a strongly coupled CFT rather than in a free theory. The hope is that studying complexity in the free theory, we can capture some of the general features which are present also in the stongly interacting CFT.

In this thesis we aim at studying complexity for the ground state of the harmonic chain with defect introduced in [62], in order to extract its divergence

pattern in the continuum limit.

Such harmonic chain with defect realises in its massless continuum limit the conformal interface described in [63]. Conformal interfaces are of great interest in modern physics [64]: they can be regarded as one-dimensional objects that connect two, possibly different, conformal field theories in two-dimensional spacetime [63, 65–69]. In condensed matter physics, they have been applied to two dimensional Ising model [65, 66], junctions of quantum wire [67–69], and to the Kondo model [70, 71]. On the other hand, they have also been largely studied in the context of the AdS/CFT correspondence, where they occur when branes extend to the boundary [63, 72–74]. Among the many applications of defects to holography, it has been recently seen that calculating holographic complexity in a defect AdS_3/CFT_2 model might shed new light in the search of the holographic dual to the complexity of the state living in the boundary quantum field theory [75]. Interestingly, it has been seen that a subleading logarithmic divergence appears in $\mathcal{CV}$ conjecture but not in $\mathcal{CA}$. In this thesis, we want to investigate if such subleading divergence is present or not in the dual quantum field theory complexity. As mentioned before, this comparison is meant to be qualitative.

Even if our main focus is complexity in presence of a defect, another quantity of great relevance in quantum information and in AdS/CFT is - as we briefly mentioned - entanglement entropy. Given a bipartite quantum mechanical system $A \cup B$ in a pure state described by the density matrix ρ, we define the reduced density matrix associated to the subsystem A as $\rho_A = \mathrm{Tr}_B\, \rho$. Then, the entanglement entropy associated to the bipartition $A \cup B$ is defined as the Von Neumann entropy of the reduced density matrix ρ_A [76, 77]:

$$S_A = -\,\mathrm{Tr}\left[\rho_A \log \rho_A\right]. \tag{1.5}$$

If we consider a CFT defined on an infinite line, the entanglement entropy of an interval of length l has a logarithmic scaling behavior at leading order [78–81]:

$$S(l) \simeq \frac{c}{3} \log\left(\frac{l}{a}\right) + \dots \tag{1.6}$$

where a is a cut-off length and c is the central charge of the model. In a CFT defined on a seminfinite line with conformally invariant boundary conditions, a similar result holds for the entanglement entropy of an interval of length l with an end on the beginning of the seminfinite line [80, 81]:

$$S(l) \simeq \frac{c}{6} \log\left(\frac{l}{a}\right) + \dots \tag{1.7}$$

Once we consider systems with defects, the entanglement entropy associated to the natural bipartition induced by a point-like defect turns out to be one of the most intriguing properties [82]. If we consider two CFTs, one defined on the half complex plane $\mathrm{Re}\, w > 0$ and the other on $\mathrm{Re}\, w < 0$, we

can put a conformal invariant defect at $\mathrm{Re}\, w = 0$ [83]. Then, the entanglement entropy of an interval of length l with an end on the defect locus, is modified replacing the central charge c in (1.6) with the coefficient $c_{eff} \in [0, c]$ [83]:

$$S(l) \simeq \frac{c_{eff}}{3} \log\left(\frac{l}{a}\right) + \dots \tag{1.8}$$

The coefficient c_{eff} depends on the features of the conformal interface: in particular, we have that $c_{eff} = 0$ for a totally reflective interface and $c_{eff} = c$ for a totally transmissive interface. It has been calculated in [62] that in the continuum limit for the critical harmonic chain defined on a segment with a defect placed in the middle, the half chain entanglement entropy is that in (1.7), up to the substitution of c with c_{eff}. This result was obtained also through numerical computations [62]. Having developed the framework to study complexity for the harmonic chain with defect, it is quite natural to repeat and extend slightly the numerical computation in [62] for the entanglement entropy of the half chain with defect. In this way, we can compare the behavior in the continuum limit of the entanglement entropy to that of complexity.

This work is organized as follows. In section 2 we revise all the necessary background for the complexity of pure state. We start with a brief review of Nielsen's approach in a quantum information framework, then we discuss the extension of complexity to a lattice quantum field theory framework and finally we revise the holographic prescriptions for the complexity of a pure state. Then, in section 3 we discuss the harmonic chain with defect introduced in [62]. In section 4, we present our numerical results for the complexity in the harmonic chain with defect. Then, in section 5, we review the result for the entanglement entropy of the half chain with defect and discuss a possible relation with the results for complexity in section 4. Finally, in section 6 we review the study of holographic complexity in presence of a defect [75] and explain how it might be related to our results. Conclusions are drawn in section 7. Moreover, some appendix, A, B and C, are present and contain either technical details or straightforward extensions of the results presented in the thesis.

2 Complexity of Pure States in Quantum Field Theory and Holography

In this section we review the fundamental concepts related to the complexity of a pure state. We start with a review of the tools developed in a quantum information framework and then discuss how to extend them to the realm of free scalar quantum field theories. Finally, we summarize the conjectures that in the recent years were made for the holographic dual of the complexity of the state defined in the boundary quantum field theory.

2.1 Complexity in Quantum Information

General Definition of Quantum Complexity The concept of complexity has been studied in quantum information for a long time [1,2]. It basically refers to the minimum number of operations which are needed to accomplish a certain task. To be more precise, in the framework of a generic quantum mechanical theory defined on the Hilbert space $\mathcal{H}$, we need to specify these four elements:

- a reference state:
$$\left|\psi_R\right\rangle \in \mathcal{H}, \tag{2.1}$$
- a target state:
$$\left|\psi_T\right\rangle \in \mathcal{H}, \tag{2.2}$$
- a set of allowed unitary operators on our quantum computer, namely the gates:
$$U_I = e^{-i\delta t \hat{K}_I}, \tag{2.3}$$
where $\hat{K}_I$ is a Hermitian operator and δt is an infinitesimal change in time.
- a tolerance cutoff:
$$\varepsilon > 0,\ \varepsilon \in \mathbb{R}. \tag{2.4}$$

Then, we define as quantum computational complexity, the minimum number of gates that are needed in order to reach target state from the reference up to the chosen tolerance:
$$\left\| \left|\psi_T\right\rangle - U \left|\psi_R\right\rangle \right\| \leq \varepsilon. \tag{2.5}$$
where
$$U = U_{I_1} U_{I_2} \dots \ . \tag{2.6}$$
It is evident that estimating complexity using directly this definition is an extremely difficult problem.

Nielsen's Approach A feasible and efficient method to approach this problem was developed by Nielsen and collaborators in [3–5]. Their idea was to visualize the problem as a Hamiltonian control problem, where the discrete string of gates in expression (2.6) is replaced by a Hamiltonian evolution:

$$U(t) = \overleftarrow{\mathcal{T}} \exp\left[-i \int_0^t d\tilde{t} H(\tilde{t})\right] \tag{2.7}$$

where $\overleftarrow{\mathcal{T}}$ is a left to right time ordering operator, $\tilde{t}$ is a time and $H(\tilde{t})$ is a Hermitian operator playing the role of the Hamiltonian of the system. In order to reproduce a circuit moving from reference $|\psi_R\rangle$ to target $|\psi_T\rangle$, we impose the following conditions:

$$U(0) = \mathbb{1}, \qquad U(1) = U_T, \qquad |\psi_T\rangle = U_T |\psi_R\rangle . \tag{2.8}$$

The Hamiltonian in equation (2.7) has the following structure:

$$H(t) = \sum_I Y_I(t) K_I, \tag{2.9}$$

where $Y_I(t)$ are the control functions determining which gate K_I is turned on at time t and the gate operators are taken as forming a basis for the space of operators to which the Hamiltonian belongs. The control functions can be regarded as the tangent vectors to the trajectory in the space of unitaries:

$$Y_I(t) K_I = \frac{dU(t)}{dt} U^{-1}(t). \tag{2.10}$$

In order to estimate the cost associated to the choice of a certain path, one can assign to each time step of the circuit a cost function [3]:

$$F(U(t), Y_I(t)), \tag{2.11}$$

for which there is no preferential choice but rather a set of desirable properties:

- smoothness:
$$F \in \mathcal{C}^\infty; \tag{2.12}$$
- positive definiteness:
$$F \geq 0 \quad \forall\, U, Y_I, \qquad F = 0 \leftrightarrow Y_I = 0; \tag{2.13}$$
- triangle inequality:
$$F(U, Y_I + \tilde{Y}_I) \leq F(U, Y_I) + F(U, \tilde{Y}_I) \quad \forall\, U, Y_I, \tilde{Y}_I; \tag{2.14}$$
- homogeneity:
$$F(U, \lambda Y_I) = \lambda F(U, Y_I) \quad \forall\, U, Y_I,\ \lambda \geq 0. \tag{2.15}$$

Some possible choices for the cost functions are:

$$F_1 = \sum_I |Y_I|, \qquad F_2 = \sqrt{\sum_I (Y_I)^2}, \quad \dots \quad F_q = \left(\sum_I (Y_I)^q\right)^{\frac{1}{q}}. \tag{2.16}$$

Then, we can define the length functional:

$$D(U) = \int_0^1 d\tilde{t} F(U(\tilde{t}), Y_I(\tilde{t})), \tag{2.17}$$

and find the path which has the minimal length. We identify complexity with the length of such optimal path. Hence the problem of finding the complexity of a certain task with a quantum computer is finally rephrased as that of finding the minimal length path, namely a geodesic in the space of unitaries. We should notice that the space of unitaries equipped with a cost function is a manifold where the length between two points is defined. Furthermore, taking F_2 cost function we obtain the structure of a standard Riemannian geometry with metric tensor $G_{IJ} = \delta_{IJ}$ and length functional:

$$D(U) = \int_0^1 d\tilde{t} \sqrt{G_{IJ} Y_I(\tilde{t}) Y_J(\tilde{t})}. \tag{2.18}$$

In this specific case, we can use all the known techniques to find geodesics to address the problem of finding complexity.

2.2 Complexity in Lattice Quantum Field Theory

Motivated by holographic conjectures for complexity, which will be described in section 2.3, several attempts were made in order to take the tools developed for complexity in quantum information and extend them to a quantum field theory framework. In this section, we review some of the key ideas developed to fulfill this task.

Set Up: Lattice of Harmonic Oscillators Given the complete lack of a quantum field theory definition for complexity, the starting point of many recent works on quantum field theory complexity [6,8], is the simplest model, i.e. the free scalar field theory in 1+1 dimensions, whose Hamiltonian defined on a segment of length $\mathcal{L}$ reads:

$$H = \frac{1}{2} \int_0^{\mathcal{L}} dx \left[\pi(x)^2 + (\partial_x \phi(x))^2 + m^2 \phi(x)^2\right], \tag{2.19}$$

where $\phi(x)$ is the scalar field and $\pi(x)$ is the conjugate momentum. These two fields satisfy the standard equal time commutation relations for quantum field theory:

$$\left[\phi(t,x), \pi(t,y)\right] = i\delta(x-y), \quad \left[\phi(t,x), \phi(t,y)\right] = 0, \quad \left[\pi(t,x), \pi(t,y)\right] = 0. \tag{2.20}$$

Since we want to use Nielsen's approach, which was developed for quantum mechanical systems with a finite number of degrees of freedom, we regard the Hamiltonian in expression (2.19) as the continuum limit of a quantum harmonic chain of coupled oscillators. For this reason, we consider a discrete version of Hamiltonian in formula (2.19), obtained placing our theory on a one dimensional lattice of spacing δ:

$$H = \frac{1}{2}\sum_{n=0}^{\mathcal{L}/\delta}\left[\frac{\pi_n^2}{\delta} + \delta\,\phi_n^2 + \frac{1}{\delta}\left(\phi_n - \phi_{n+1}\right)^2\right], \tag{2.21}$$

where ϕ_n and π_n are the fields calculated in the space point $x = n\delta$. Through some simple identifications,

$$x_n = \delta^{\frac{1}{2}}\phi_n, \quad p_n = \frac{\pi_n}{\delta^{\frac{1}{2}}}, \quad M = \frac{1}{\delta}, \quad \Omega_0 = m, \quad K = \frac{1}{\delta}, \tag{2.22}$$

we can show that the lattice quantum field theory Hamiltonian is perfectly equivalent to a quantum mechanical Hamiltonian of a system of coupled harmonic oscillators:

$$H = \frac{1}{2}\sum_{n=0}^{N}\left[\frac{p_n^2}{M} + M\Omega_0^2 x_n^2 + K\left(x_n - x_{n+1}\right)^2\right], \tag{2.23}$$

where the two dynamical variables satisfy the usual canonical commutation relations,

$$\left[x_i, p_j\right] = i\delta_{ij} \quad \left[x_i, x_j\right] = 0 \quad \left[p_i, p_j\right] = 0, \tag{2.24}$$

which in the continuum limit give the canonical commutation relations in formula (2.20).

Ground State Complexity of a Lattice of Coupled Harmonic Oscillators The first approach to complexity in a lattice quantum field theory framework was developed in [6], where the complexity associated to the ground state of the harmonic chain of oscillators in formula (2.23) is computed. The reference state is taken to be the maximally unentangled state, defined as the ground state of a chain of decoupled oscillators of mass parameter ω_0:

$$H = \frac{1}{2}\sum_{n=1}^{N}\left[p_n^2 + \omega_0^2 x_n^2\right]. \tag{2.25}$$

Periodic boundary conditions are taken for both Hamiltonians in expressions (2.23) and (2.25). In terms of wavefunctions, we have that the target and reference state read:

$$\psi_{T,R} = \left(\frac{\det A_{T,R}}{\pi}\right)^{\frac{1}{4}} \exp\left[-\frac{1}{2}x^T A_{T,R} x\right] \qquad x = \left(x_1, x_2, \dots\right)^T, \tag{2.26}$$

where we have that:

$$A_R = \omega_0 \mathbb{1}, \qquad A_T = \begin{bmatrix} \Omega_0^2 + 2K & K & & & \\ K & \Omega_0^2 + 2K & K & & \\ & K & \Omega_0^2 + 2K & \ddots & \\ & & \ddots & \ddots & \end{bmatrix}. \tag{2.27}$$

We introduce the normal mode basis $\tilde{x}$ and $\tilde{p}$ where the matrices $\tilde{A}_T$ and $\tilde{A}_R$ are both in a diagonal form:

$$\tilde{A}_R = \omega_0 \mathbb{1}, \qquad \tilde{A}_T = \begin{bmatrix} \tilde{\omega}_0 & & & \\ & \tilde{\omega}_1 & & \\ & & \tilde{\omega}_2 & \\ & & & \ddots \end{bmatrix}, \tag{2.28}$$

with:

$$\tilde{\omega}_n^2 = \Omega_0^2 + 4K \sin^2 \frac{\pi n}{N} \qquad n \in \{0, 1, \ldots, N-1\}. \tag{2.29}$$

At this point, we ask ourselves what is the complexity associated to this family of quantum circuits:

$$\gamma \colon \psi_R \to \psi_T. \tag{2.30}$$

In [6] the first cost function which is considered is the F_2 cost function, which, as explained at the end of section 2.1, gives to the space of unitary transformations the structure of a Riemannian manifold with metric tensor $G_{IJ} = \delta_{IJ}$. However, identifying control functions Y_I by writing equation (2.10) using a basis of the unitary operators acting directly on wavefunctions makes the problem intractable. For this reason the authors of [6] decided to restrict to the subspace of states whose wavefunction has the form described in equation (2.26) where the matrices $A_{T,R}$ are replaced by a generic matrix A real and positive definite. For this peculiar class of states we can trade the wavefunctions for such matrices A, which completely and uniquely characterize our state:

$$\psi(x) = \left(\frac{\det A}{\pi}\right)^{\frac{1}{4}} \exp\left[-\frac{1}{2} x^T A x\right] \longleftrightarrow A \textit{ real and positive.} \tag{2.31}$$

It is possible to rewrite the quantum circuits that remain within this subspace of states, as linear operators $G(\tilde{t}) \in GL(N, \mathbb{R})$ acting on the matrices A:

$$\tilde{A}_T = G(\tilde{t} = 1) \tilde{A}_R G^T(\tilde{t} = 1). \tag{2.32}$$

Among all the possible paths of the form described above, the optimal one has been proved in [6] to be the straight line circuit, which directly amplifies

the normal modes $\omega_0 \to \tilde{\omega}_n$. For such optimal path, the operator G takes the form:

$$G(\tilde{t}) = \exp\left[\tilde{M}_0 \tilde{t}\right] \quad \tilde{M}_0 = diag\left(\frac{1}{2}\log\frac{\tilde{\omega}_0}{\omega_0}, \frac{1}{2}\log\frac{\tilde{\omega}_1}{\omega_0}, \ldots, \frac{1}{2}\log\frac{\tilde{\omega}_{N-1}}{\omega_0}\right). \tag{2.33}$$

This result was shown to hold not only for F_2 but for also for F_1 and all the F_q cost functions in formula (2.16). At this point, all that remains is to find the control functions $Y_I(t)$, which are useful to calculate complexity. With this purpose, we notice that it is possible to rewrite equations (2.8) and (2.10) in a version restricted to the $GL(N,\mathbb{R})$ matrices acting on the A matrices:

$$G(\tilde{t}) = \overleftarrow{\mathcal{T}} \exp\left[-i\int_0^t d\tilde{t} \sum_I Y_I(t) M_I\right], \qquad Y_I(t) M_I = \frac{dG(t)}{dt} G^{-1}(t), \tag{2.34}$$

where $\{M_I\}_I$ form a basis for $GL(N,\mathbb{R})$, which is formed by the matrices having one entry equal to one and all the other entries null:

$$M_1 = \begin{bmatrix} 1 & 0 & \cdots \\ 0 & 0 & 0 \\ \vdots & 0 & \ddots \end{bmatrix}, \quad M_2 = \begin{bmatrix} 0 & 1 & \cdots \\ 0 & 0 & 0 \\ \vdots & 0 & \ddots \end{bmatrix}, \quad \ldots \tag{2.35}$$

Given the form of the optimal path, we can calculate control functions along it by reverting the last equation in formula (2.34):

$$Y_I(\tilde{t}) = \mathrm{Tr}\left[\partial_{\tilde{t}} G(\tilde{t}) G^{-1}(\tilde{t}) M_I^T\right] \implies Y_I(\tilde{t}) \equiv \frac{1}{2}\log\frac{\tilde{\omega}_I}{\omega_0}. \tag{2.36}$$

Then the results for the complexity of the ground state of the harmonic chain of oscillators can be straightforwardly derived computing the integral in formula (2.17) along the optimal path:

$$\mathcal{C}_1 = \sum_i \left|\log\frac{\tilde{\omega}_i}{\omega_0}\right|, \quad \mathcal{C}_2 = \frac{1}{2}\sqrt{\sum_i \left(\log\frac{\tilde{\omega}_i}{\omega_0}\right)^2}, \quad \mathcal{C}_q = \frac{1}{2^q}\left(\sum_i \left(\log\frac{\tilde{\omega}_i}{\omega_0}\right)^q\right)^{\frac{1}{q}}. \tag{2.37}$$

Covariance Matrix Formalism for the Complexity of Gaussian States The covariance formalism is a powerful tool which allows us to find a simple and rather elegant formula - see equation (2.60) - for the complexity of a generic Gaussian state with N bosonic degrees of freedom, provided that we specialize our discussion to F_2 cost function. The first example of application of the covariance matrix formalism to complexity is given in [8], to which we will refer in our subsequent calculations. First of all, we consider the Hamiltonian

in formula (2.23), whose dominion is contained in the Hilbert space of N harmonic oscillator and focus on the pure Gaussian states. We define a Gaussian state as that which has the most general Gaussian wavefunction:

$$\psi(x_i) = \sqrt[4]{\det \frac{A}{\pi}} \exp\left[-\frac{1}{2} x_i (A_{ij} + iB_{ij}) x_j\right], \tag{2.38}$$

where A and B are real bilinear forms and A is positive defined. We should notice that such states represent a more general class of pure states than the one considered in [6] and described in expression (2.31), which is reobtained imposing the constraint $B = 0$. Those states are completely characterized by the two point function of positions and momenta. Storing positions and momenta together into a compact vector,

$$r_i = \left(x_1, \ldots, x_N, p_1, \ldots, p_N\right), \tag{2.39}$$

we can express the two point function in terms of its symmetric and antisymmetric part, respectively G_{ij} and J_{ij}:

$$\langle \psi | r_i r_j | \psi \rangle = \frac{1}{2}\left(G_{ij} + iJ_{ij}\right). \tag{2.40}$$

Imposing the canonical commutation relations for a bosonic Gaussian state

$$[r_i, r_j] = iJ_{ij} \qquad J = \begin{bmatrix} 0 & \mathbb{1} \\ -\mathbb{1} & 0 \end{bmatrix}, \tag{2.41}$$

we notice that the antisymmetric part of the two point function is completly fixed to be equal to the symplectic unit. We conclude that the Gaussian pure state of a bosonic system made of N modes is completely and uniquely identified by the symmetric part of its two point functions , G_{ij}, which is the *bosonic covariance matrix*. At this point we wish to characterize the subgroup of unitary transformations mapping a pure bosonic Gaussian state into another pure bosonic Gaussian state, namely the Bogoliubov transformations. We consider $\hat{K}$ to be the quadratic form generating such subgroup:

$$\hat{K} = \frac{1}{2} r_i k_{ij} r_j, \tag{2.42}$$

and take k_{ij} to be a real symmetric form. The operator $\hat{K}$ generates the unitary transformation $\hat{U}(\tilde{t})$ which acts on Gaussian pure states as follows:

$$\hat{U}(\tilde{t}) = e^{-i\tilde{t}\hat{K}}, \quad \left|G_{\tilde{t}}\right\rangle = \hat{U}(\tilde{t}) \left|G_0\right\rangle, \tag{2.43}$$

and changes positions and momenta in this way:

$$\hat{U}(\tilde{t})^\dagger \, r_i \, \hat{U}(\tilde{t}) = \sum_{n=0}^{\infty} \frac{\tilde{t}^n}{n!} \left[i\hat{K}, r_i\right]_{(n)}, \tag{2.44}$$

where we used Baker-Campbell-Hausdorff formula and defined recursively this operation:

$$[i\hat{K}, r_i]_{(0)} = r_i \qquad [i\hat{K}, r_i]_{(n)} = [i\hat{K}, [i\hat{K}, r_i]_{(n-1)}]. \tag{2.45}$$

We can read off the matricial form K of the generator $\hat{K}$:

$$K_{ij} = J_{in} k_{nj} \tag{2.46}$$

by simply applying the canonical commutation relation to the following commutator:

$$[i\hat{K}, r_i] = J_{in} k_{nj} r_j. \tag{2.47}$$

Then we can write the matricial transformation $U(\tilde{t})$ generated by K as follows:

$$U(\tilde{t}) = e^{\tilde{t}K} \rightsquigarrow \hat{U}^{\dagger}(\tilde{t})\ r_i\ \hat{U}(\tilde{t}) = U(\tilde{t}) r_i \qquad . \tag{2.48}$$

We still have to impose that the operator $U(\tilde{t})$ satisfies the canonical commutation relations, i.e. that it preserves the symplectic unit J:

$$U(\tilde{t}) J U(\tilde{t})^T = J. \tag{2.49}$$

This leads to the condition for the generator K:

$$KJ + JK^T = 0, \tag{2.50}$$

and definitely tells us that the group of unitary transformations mapping Gaussian states into Gaussian states is the $2N$ dimensional symplectic group:

$$U(\tilde{t}) \in Sp(2N, \mathbb{R}), \qquad K \in \mathfrak{sp}(2N, \mathbb{R}). \tag{2.51}$$

At this point it is possible to rewrite the quantum circuit remaining within the subspace of Gaussian states in terms of the operators $U(\tilde{t})$ acting on the covariance matrices G:

$$\begin{aligned} G_{ij}(\tilde{t}) &= \big\langle G(\tilde{t}) \big| (r_i r_j + r_j r_i) \big| G(\tilde{t}) \big\rangle = \\ &= \big\langle G(0) \big| e^{i\tilde{t}\hat{K}} (r_i r_j + r_j r_i) e^{-i\tilde{t}\hat{K}} \big| G(0) \big\rangle \\ &= U(\tilde{t})_{in}\ U(\tilde{t})_{mj}\ \big\langle G(0) \big| (r_n r_m + r_m r_n) \big| G(0) \big\rangle \\ &= U(\tilde{t})_{in}\ G_{nm}(0)\ U(\tilde{t})_{mj}. \end{aligned} \tag{2.52}$$

and specialize to the the family of trajectories connecting reference and target states:

$$G(\tilde{t}) = U(\tilde{t}) G_R U(\tilde{t})^T \quad \tilde{t} \in [0, 1], \tag{2.53}$$

where:

$$U(0) = \mathbb{1} \quad G_T = U(1) G_R U(1)^T. \tag{2.54}$$

The operator $U(\tilde{t})$ defines the action of all the steps in the quantum circuit up to time $\tilde{t}$ and can be regarded as:

$$U(\tilde{t}) = \overleftarrow{\mathcal{T}} \exp \int_0^t d\tilde{t} K(\tilde{t}) \qquad K(\tilde{t}) = Y_I(\tilde{t}) K_I, \tag{2.55}$$

where $\{K_I\}_I$ forms a basis of generators of $\mathfrak{sp}(2N, \mathbb{R})$. We can easily notice the presence of an ambiguity: the transformation $U(\tilde{t})$ is defined up to the stabilizer group, which is the subgroup of $Sp(2N, \mathbb{R})$ preserving the covariance matrix of the reference state and in our case corresponds to $U(N)$:

$$Sta_{G_R} = \{U_R \in Sp(2N, \mathbb{R}) \mid U_R G_R U_R^T = G_R\} \simeq U(N). \tag{2.56}$$

In order to eliminate this ambiguity, we define the relative covariance matrix Δ, which expresses the relation between the target and reference covariance matrices in a basis independent way:

$$\Delta = G_T G_R^{-1}. \tag{2.57}$$

Hence, every quantity that is invariant under $Sp(2N, \mathbb{R})$ group is necessarily a pure function of Δ. Once established the form for a quantum circuit connecting the two Gaussian states as that of expression (2.55), we address the problem of finding the minimal length functional for a given cost function. We recall that the F_2 cost function is such that it equips the $Sp(2N, \mathbb{R})$ group with a Riemannian metric of this form:

$$ds^2 = \frac{1}{2} \mathrm{Tr}\Big(dU U^{-1} G_T (dU U^{-1})^T G_R^{-1}\Big) = \frac{1}{2} \mathrm{Tr}\Big(K(\tilde{t}) G_T K(\tilde{t})^T G_R^{-1}\Big) d\tilde{t}^2. \tag{2.58}$$

Now all that is left is the problem of finding the geodesic connecting reference and target in such Riemannian manifold. The authors of [8] managed to prove with Lie group techniques that the optimal path connecting two generic Gaussian states can be expressed in terms of the relative covariance as follows:

$$\gamma := U(\tilde{t}) = e^{\frac{\tilde{t}}{2} \log \Delta}. \tag{2.59}$$

This yields an elegant formula for $\mathcal{C}_2$ complexity:

$$\mathcal{C}_2 = \frac{1}{2\sqrt{2}} \sqrt{\mathrm{Tr}\left[(\log \Delta)^2\right]}. \tag{2.60}$$

2.3 Complexity in Holography

In this section we review the main conjectures related to the gravitational observable dual to quantum field theory complexity for the state living in the boundary. The two proposals at play are the so-called *complexity equals volume* ($\mathcal{CV}$) and *complexity equals action* ($\mathcal{CA}$).

Complexity equals Volume The conjecture *complexity equals volume* was formulated by Susskind and collaborators in [52,55]. It states that the complexity associated to the quantum field theory state living on the boundary is dual to the maximal volume codimension-one bulk surface anchored at the time slice Σ living in the asymptotic boundary where the state is defined:

$$C_V = \max_{\Sigma=\partial\mathcal{B}} \left[\frac{\mathcal{V}(\mathcal{B})}{G_N L} \right]. \tag{2.61}$$

with $\mathcal{B}$ corresponding to the bulk hypersurface of interest, G_N to the Newton's constant of the bulk gravitational theory and L to the curvature radius of AdS geometry. It is important to stress that in this conjecture the quantum state in the boundary is assumed to be a pure state. What led Susskind and collaborators to elaborate $\mathcal{CV}$ is the observation that the almost linear growth at late time of the Einstein-Rosen bridge cannot be adequately probed by holographic entanglement entropy [84]. Hence, they hypothesized that such linear growth could be considered in analogy to the corrsponding property of the complexity of the quantum state living in the boundary. We can see that the prescription in formula (2.61) reproduces such late time linear growth in the case of the eternal AdS black hole in d+1 dimensions, described by the following metric:

$$ds^2 = -f(r)dt^2 + \frac{dr^2}{f(r)} + r^2 d\Sigma^2_{k,d-1}, \quad f(r) = k + \frac{r^2}{L^2} - \frac{\omega^{d-2}}{r^{d-2}}, \tag{2.62}$$

where $k \in 0, \pm 1$ is the curvature of the (d-1)-dimensional line element $d\Sigma^2_{k,d-1}$ and ω is related to the position of the black hole horizon:

$$\omega^{d-2} = r_h^{d-2}\left(k + \frac{r_h^2}{L^2}\right). \tag{2.63}$$

In [85–87], complexity has been calculated for such black hole using the $\mathcal{CV}$ prescription and it has been shown that:

$$\frac{d\mathcal{C}}{dt} = -\frac{\Omega_{k,d-1}}{G_N L} E, \tag{2.64}$$

where E is a conserved quantity and $\Omega_{k,d-1}$ is the dimensionless volume of the $(d-1)$-dimensional spatial geometry. In particular in [55,87], it has been seen that in the case of a planar AdS black hole (k=0) complexity is such that:

$$\frac{d\mathcal{C}}{dt}|_{t\to\infty} = \frac{8\pi}{d-1} M, \tag{2.65}$$

where M is the mass of the black hole. This clearly hints that the observable we defined as the holographic dual of complexity exhibits a late time linear growth, which constitutes an argument in favor of $\mathcal{CV}$ conjecture.

Complexity equals Action The conjecture *complexity equals action* ($\mathcal{CA}$) has been formulated in [58,59]. It tells that the complexity is proportional to the gravitational action evaluated on the Wheeler-DeWitt (WDW) patch, which is defined as the union of all spacelike surfaces anchored at the boundary time slice where the quantum state lives:

$$\mathcal{C}_A = \frac{I_{WDW}}{\pi}. \tag{2.66}$$

It is evident that the spacelike region corresponding to WDW patch may have a very complicate shape, and therefore it might be difficult to evaluate on it the gravitiational action. In [88], we can find the prescriptions for the precise evaluation of the action integral on WDW patch, whose general form is written below,

$$I_{WDW} = I_{EH} + I_{GHY} + I_{NULL} + I_{CT} + I_{JOINTS}, \tag{2.67}$$

and contains all those terms:

- I_{EH} is the bulk Einstein-Hilbert action;
- I_{GHY} is the Gibbons-Hawking-York action for timelike and spacelike boundaries of WDW patch;
- I_{NULL} is the action on null boundaries of WDW patch;
- I_{CT} is the counterterm introduced to ensure parametrization invariance of I_{NULL};
- I_{JOINTS} is the action calculated at the intersections of two surfaces at the boundary of the WDW patches.

We do not enter into further technical details, which can be found in [88], because it would be out of the scope of this project. Finally, we just recall that the late time linear growth, which is expected to be a general feature of complexity, is recovered also with $\mathcal{CA}$ prescription in the framework of the eternal black hole described by metric in formula (2.62). In fact, in [87], it has been shown that complexity associated to such black hole in $\mathcal{CA}$ conjecture is such that at late time it grows linearly in this way:

$$\frac{d\mathcal{C}_A}{dt}|_{t\to\infty} = \frac{2M}{\pi}, \tag{2.68}$$

where M is taken to be the black hole mass. This is a sign that $\mathcal{CA}$ can be taken as an equivalently good conjecture to describe the gravitational dual of quantum field theory complexity.

3 The Harmonic Chain with Defect

In this section we describe the set up to be considered in our calculations for $\mathcal{C}_2$ complexity. We first describe the harmonic chain with defect introduced in [62] and discuss the possible boundary conditions. We then proceed to discuss the diagonalization of its Hamiltonian and finally we compute momentum and position correlators to be used in the calculations of complexity for the Gaussian states.

3.1 Harmonic Chain with Defect on a Segment

Chain on the Segment We consider the harmonic chain which is introduced in [62], whose Hamiltonian is defined on a segment, is made of $2L$ sites and contains a scale invariant defect. It reads:

$$\begin{aligned} H = &\sum_{n=1}^{L}\left(\frac{p_n^2}{2m_1}+\frac{1}{2}m_1\Omega_0^2x_n^2\right)+\sum_{n=1}^{L-1}\left(\frac{m_1}{2}(x_n-x_{n+1})^2\right)+\\ &+\frac{1}{2}K_0(x_L-x_{L+1})^2+\\ &+\sum_{n=L+1}^{2L}\left(\frac{p_n^2}{2m_2}+\frac{1}{2}m_2\Omega_0^2x_n^2\right)+\sum_{n=L+1}^{2L-1}\left(\frac{m_1}{2}(x_n-x_{n+1})^2\right), \end{aligned} \tag{3.1}$$

where Ω_0 is the mass of the chain in the limit where the defect is absent and m_1, m_2 and K_0 are all parameters dependent on the so called defect strength $\theta \in \mathbb{R}$:

$$m_1 = e^{\theta} \quad m_2 = e^{-\theta} \quad K_0 = \left[\frac{1}{2}\left(\frac{1}{m_1}+\frac{1}{m_2}\right)\right]^{-1} = \frac{1}{\cosh\theta}. \tag{3.2}$$

We have that the canonical commutation relations hold:

$$\Big[x_i, p_j\Big] = i\delta_{ij} \quad \Big[x_i, x_j\Big] = 0 \quad \Big[p_i, p_j\Big] = 0. \tag{3.3}$$

For reasons which will be more clear at the end of this section, we will call this set of coordinates, as *Extended Coordinates*. The intuitive argument is that the effect of changing the parameter θ in this coordinate system is two sided: on one hand it modifies the spring constant K_0 in the locus of defect, and on the other, it is spread throughout the chain because of m_1 and m_2.

Boundary Conditions We notice that the harmonic chain in [62] is such that no interaction with the walls occurs, as it is pictorially represented in figure 4. This means that in the continuum limit we obtain a quantum field theory defined on segment with Hamiltonian in formula (2.19) with von Neumann boundary conditions:

$$\partial_x\Phi(t,\vec{x})|_{x=0,\mathcal{L}} = \partial_x\Pi(t,\vec{x})|_{x=0,\mathcal{L}} = 0. \tag{3.4}$$

However, if we wanted, we could easily extend our discussion to the case where chain is attached to two rigid walls, i.e where Dirichlet boundaries, $q_0 = q_{2L+1} = 0$ and $p_0 = p_{2L+1} = 0$, are imposed. This situation is pictorially represented in figure 5. Notice that the only difference between the two cases consists in the interaction with the fixed boundaries, which would result in a slight change in the spectrum and the eigenfunctions but not in the structure of the problem.

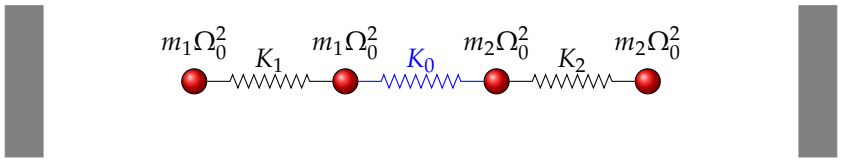

Figure 4: Harmonic Chain with Defect.No Boundary Conditions.

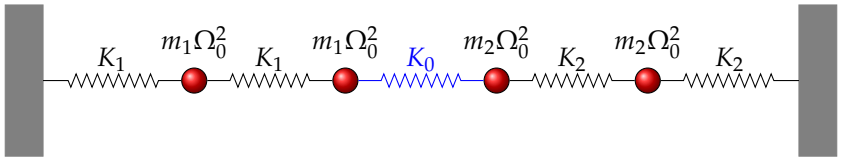

Figure 5: Harmonic Chain on a Segment.Dirichlet Boundary Conditions.

Scale Invariance We have that this choice of the parameters implies that the spectrum of our chain is scale invariant: in fact, we have that the spectrum depends on the ratio between the spring constants and the parameter m_i with $i = 1, 2$. On the left and right side we have that the spring constants are respectively m_1 and m_2, and such ratio is equal to one. On the contact point instead, we have to compare the spring constant K_0 with the reduced mass m_{red}:

$$m_{red} = 2\left(\frac{1}{m_1} + \frac{1}{m_2}\right)^{-1} \rightsquigarrow \frac{K_0}{m_{red}} = 1. \tag{3.5}$$

Localized Coordinates We can look at the problem in a different coordinate system. We may absorb m_1 and m_2 in the dynamical variables through a canonical transformation:

$$\begin{cases} p_i \longrightarrow \frac{p_i}{\sqrt{m_1}} & i \in 1, \dots, L \\ p_i \longrightarrow \frac{p_i}{\sqrt{m_2}} & i \in L+1, \dots, 2L \end{cases} \quad \begin{cases} q_i \longrightarrow q_i\sqrt{m_1} & i \in 1, \dots, L \\ q_i \longrightarrow q_i\sqrt{m_2} & i \in L+1, \dots, 2L \end{cases}, \tag{3.6}$$

which can be easily seen to be canonical and to bring the Hamiltonian in equation (3.1) into the following form:

$$\begin{aligned} H = &\sum_{n=1}^{L}\left(\frac{p_n^2}{2}+\frac{1}{2}\Omega_0^2 x_n^2\right)+\sum_{n=1}^{L-1}\left(\frac{1}{2}(x_n-x_{n+1})^2\right)+ \\ &+\frac{1}{2}\frac{K_0}{m_1}x_L^2+\frac{1}{2}\frac{K_0}{m_2}x_{L+1}^2-K_0 x_L x_{L+1} \\ &+\sum_{n=L+1}^{2L}\left(\frac{p_n^2}{2}+\frac{1}{2}\Omega_0^2 x_n^2\right)+\sum_{n=L+1}^{2L-1}\left(\frac{1}{2}(x_n-x_{n+1})^2\right). \end{aligned} \tag{3.7}$$

We can rewrite the Hamiltonian in equation (3.7) using a matricial notation:

$$H=\frac{1}{2}\vec{p}\cdot\vec{p}+\frac{1}{2}\vec{x}\cdot\mathcal{V}\vec{x} \tag{3.8}$$

where:

$$\mathcal{V}=\begin{bmatrix} \Omega_0^2+1 & -1 & & & & & & & & & & \\ -1 & \Omega_0^2+2 & -1 & & & & & & & & & \\ & -1 & \Omega_0^2+2 & \ddots & & & & & & & & \\ & & \ddots & \ddots & -1 & & & & & & & \\ & & & -1 & \Omega_0^2+\frac{K_0}{m_1}+1 & -K_0 & & & & & & \\ & & & & -K_0 & \Omega_0^2+\frac{K_0}{m_1}+1 & -1 & & & & & \\ & & & & & -1 & \ddots & \ddots & & & & \\ & & & & & & \ddots & \Omega_0^2+2 & -1 & & & \\ & & & & & & & & \Omega_0^2+2 & -1 & & \\ & & & & & & & & -1 & \Omega_0^2+1 & & \\ & & & & & & & & & & & \end{bmatrix}. \tag{3.9}$$

Since $\mathcal{C}_2$ complexity is in general basis dependent, we will study it in both coordinate system: we will call the first one as *Extended Coordinates* whereas the other coordinates will be named *Localized Coordinates*. The reason for introducing this new coordinate system is that if we change θ, this affects only the spring constant and the mass parameters near the defect locus.

3.2 Spectrum of the Harmonic Chain with Defect

We first analyze the spectrum of the harmonic chain with defect defined on a segment, following the methods developed in [62]. Since the change of basis in formula (3.6) is canonical, we might refer equivalently to the Hamiltonian in formula (3.1) or to that in formula (3.7).

Homogeneous Problem In order to find the spectrum of the model, we first look at the problem for the homogeneous chain, where the matrix to be

diagonalized is given by the no defect limit of the matrix in (3.9):

$$\mathcal{V}_{Hom} = \begin{bmatrix} \Omega_0^2+1 & -1 & & & & & & & & & \\ -1 & \Omega_0^2+2 & -1 & & & & & & & & \\ & -1 & \Omega_0^2+2 & \ddots & & & & & & & \\ & & \ddots & \ddots & -1 & & & & & & \\ & & & -1 & \Omega_0^2+2 & -1 & & & & & \\ & & & & -1 & \Omega_0^2+2 & -1 & & & & \\ & & & & & -1 & \ddots & \ddots & & & \\ & & & & & & \ddots & \Omega_0^2+2 & -1 & & \\ & & & & & & & & \Omega_0^2+2 & -1 & \\ & & & & & & & & -1 & \Omega_0^2+1 \end{bmatrix}. \tag{3.10}$$

Following [62], we see that the eigenvalues of the homogeneous problem are:

$$\Omega_m^{2\ hom} = \Omega_0^2 + 2\left(1 - \cos\frac{(m-1)\pi}{2L}\right) \qquad m \in 1,\dots,2L, \tag{3.11}$$

whereas the eigenfunctions are:

$$\Phi_m^{hom}(n) = \sqrt{\frac{1}{2L}} \qquad m = 1,\ n \in 1,\dots,2L, \tag{3.12}$$

$$\Phi_m^{hom}(n) = \sqrt{\frac{1}{L}}\cos\frac{(n-\frac{1}{2})(m-1)\pi}{2L} \qquad m \in 2,\dots,2L,\ n \in 1,\dots,2L. \tag{3.13}$$

Inhomogeneous Problem We now wish to move to the inhomogeneous problem. Following [62], we make the ansatz that the spectrum remains the same:

$$\Omega_m = \Omega_m^{hom}, \tag{3.14}$$

whereas the eigenfunctions are modified with a defect dependent factor:

$$\Phi_m(n) = \begin{cases} \alpha_m \Phi_m^{hom}(n) & n \in 1,\dots,L \\ \beta_m \Phi_m^{hom}(n) & n \in L+1,\dots,2L \end{cases} \qquad \alpha_m \in \mathbb{R},\ \beta_m \in \mathbb{R}. \tag{3.15}$$

We can find α_m and β_m requiring two conditions:

- Orthonormality of the Eigenfunctions:

$$\sum_{j=1}^{2L} \Phi_m(j)\Phi_n(j) = \delta_{nm}, \tag{3.16}$$

  which implies that:

$$[\alpha_m\alpha_n + (-)^{m+n}\beta_m\beta_n] \sum_{j=1}^{L} \Phi_m^{hom}(j)\Phi_n^{hom}(j) = \delta_{mn}. \tag{3.17}$$

- Eigenvalue equations at the defect interface:

$$\begin{bmatrix} -1 & \Omega_0^2 + \frac{K_0}{m_1} + 1 & -K_0 & 0 \\ 0 & -K_0 & \Omega_0^2 + \frac{K_0}{m_1} + 1 & -1 \end{bmatrix} \begin{bmatrix} \alpha_m \Phi_m^{hom}(L-1) \\ \alpha_m \Phi_m^{hom}(L) \\ \beta_m \Phi_m^{hom}(L+1) \\ \beta_m \Phi_m^{hom}(L+2) \end{bmatrix} = \Omega_m^{hom} \begin{bmatrix} \alpha_m \Phi_m^{hom}(L) \\ \beta_m \Phi_m^{hom}(L+1) \end{bmatrix}, \tag{3.18}$$

  which implies that:

$$\alpha_m \beta_m = K_0 = \frac{1}{\cosh \theta}. \tag{3.19}$$

Solving the constraints given by equations (3.17) and (3.19), we find that:

$$\alpha_m^2 = 1 + (-)^{m+1} \tanh \theta \qquad m \in \{1, \dots, L\}, \tag{3.20}$$

$$\beta_m^2 = 1 + (-)^m \tanh \theta \qquad m \in \{L+1 \dots 2L\}. \tag{3.21}$$

Solving the Orthonormality Condition We now focus on the derivation of equation (3.17). First, we rewrite the orthonormality condition in formula (3.16) as follows:

$$\alpha_n \alpha_m A_{nm} + \beta_n \beta_m B_{nm} = \delta_{nm}, \tag{3.22}$$

where:

$$A_{nm} = \sum_{j=1}^{L} \Phi_m^{hom}(j) \Phi_n^{hom}(j) \qquad B_{nm} = \sum_{j=L+1}^{2L} \Phi_m^{hom}(j) \Phi_n^{hom}(j). \tag{3.23}$$

We may exploit the reflection symmetry with respect to the defect point of the harmonic chain defined on a segment and find that:

$$\Phi_m^{hom}(2L - j) = (-)^{m-1} \Phi_m^{hom}(j) \implies B_{nm} = (-)^{n+m} A_{nm}. \tag{3.24}$$

This leads to:

$$\left(\alpha_n \alpha_m + (-)^{n+m} \beta_n \beta_m \right) A_{nm} = \delta_{nm}, \tag{3.25}$$

where A_{nm} can be evaluated as follows:

$$A_{nm} = \begin{cases} \frac{1}{2} & n = m \\ 0 & m - n \neq 0, \ even \\ \frac{1}{4L} \left[\frac{\sin\left(\frac{\pi}{2}(m-n)\right)}{\sin\left(\frac{\pi}{4L}(m-n)\right)} \right] & m - n \neq 0, \ odd \end{cases}. \tag{3.26}$$

Solving the Eigenvalue Equations on Defect Interface Finally, we specialize our discussion to the derivation of the constraint in equation (3.19). Given the ansatz in expression (3.14), we consider the homogeneous eigenvalue equations:

$$\Omega_m^{hom} \Phi_m^{hom}(L) = \begin{bmatrix} -1 & \Omega_0^2 + 2 & -1 \end{bmatrix} \begin{bmatrix} \Phi_m^{hom}(L-1) \\ \Phi_m^{hom}(L) \\ \Phi_m^{hom}(L+1) \end{bmatrix}, \tag{3.27}$$

$$\Omega_m^{hom}\Phi_m^{hom}(L+1) = \begin{bmatrix} -1 & \Omega_0^2+2 & -1 \end{bmatrix} \begin{bmatrix} \Phi_m^{hom}(L) \\ \Phi_m^{hom}(L+1) \\ \Phi_m^{hom}(L+2) \end{bmatrix}, \tag{3.28}$$

and we plug them in equation (3.18), getting that:

$$\begin{bmatrix} \left(\frac{K_0}{m_1}\right)\alpha_n & \alpha_n - K_0\beta_n \\ \beta_n - K_0\alpha_n & \left(\frac{K_0}{m_2}\right)\beta_n \end{bmatrix} \begin{bmatrix} \Phi_m^{hom}(L) \\ \Phi_m^{hom}(L+1) \end{bmatrix} = 0. \tag{3.29}$$

We impose the condition that the determinant of the matrix of the above equation is null and obtain that:

$$-2\alpha_n\beta_n + K_0(\beta_n^2 + \alpha_n^2) = 0. \tag{3.30}$$

We use equation (3.25) in the case where $n = m$, to find that:

$$\alpha_n^2 + \beta_n^2 = 2 \implies \alpha_n\beta_n = K_0. \tag{3.31}$$

3.3 Second Quantization for the Harmonic Chain with Defect

We wish to transform the Hamiltonian in equations (3.7) and (3.8) into the Hamiltonian of a chain of decoupled oscillators, through a canonical transformation. Then, we wish to define a second quantization Hamiltonian as in equation (3.36) and to find the change of basis connecting our dynamical variables to second quantization operators.

Structure of the Orthogonal Change of Basis We wish to define the orthogonal matrix $P_{ij}(\theta)$, which induces the following change of basis:

$$\begin{bmatrix} \tilde{\vec{x}} \\ \tilde{\vec{p}} \end{bmatrix} = \begin{bmatrix} P(\theta)^T & 0 \\ 0 & P(\theta)^T \end{bmatrix} \begin{bmatrix} \vec{x} \\ \vec{p} \end{bmatrix}, \tag{3.32}$$

such that:

- it is canonical;
- it reshapes the Hamiltonian of our problem in this way:

$$\begin{aligned} H &= \frac{1}{2}\vec{p}\cdot\vec{p} + \frac{1}{2}\vec{x}\cdot\mathcal{V}\vec{x} = \\ &= \frac{1}{2}(P(\theta)^T\vec{p})\cdot(P(\theta)^T\vec{p}) + \frac{1}{2}(P(\theta)^T\vec{x})\cdot \underbrace{P(\theta)^T\mathcal{V}P(\theta)}_{Diag(\Omega_1^2,\dots\Omega_{2L}^2)} P(\theta)^T\vec{x} = \\ &= \frac{1}{2}\sum_{i=1}^{2L}\left(\tilde{p}_i^2 + \Omega_i^2\tilde{x}_i\right). \end{aligned} \tag{3.33}$$

If we consider the Hamiltonian in the Localized Basis in (3.7), the matrix $P(\theta)$, containing on the columns the eigenvectors, has the following form:

$$P_{ij}(\theta) = \mathcal{D}_{ij}(\theta)\Phi_j^{hom}(i). \tag{3.34}$$

The coefficient $\mathcal{D}_{ij}(\theta)$ encloses the dependence from the defect and takes this form:

$$\mathcal{D}_{ij}(\theta) = \begin{cases} \sqrt{1+(-)^{j+1}\tanh\theta} & i \in \{1,\dots,L\} \\ \sqrt{1+(-)^{j}\tanh\theta} & i \in \{L+1\dots 2L\} \end{cases}. \tag{3.35}$$

Second Quantization Hamiltonian At this point is possible to write the Hamiltonian above in terms of the second quantization operators:

$$H = \sum_{i=1}^{2L} \Omega_i \left(\hat{a}_i^\dagger \hat{a}_i + \frac{1}{2}\right), \tag{3.36}$$

where:

$$\hat{a}_i = \sqrt{\frac{\Omega_i}{2}}\left(\tilde{x}_i + i\frac{\tilde{p}_i}{\Omega_i}\right), \qquad \hat{a}_i^\dagger = \sqrt{\frac{\Omega_i}{2}}\left(\tilde{x}_i - i\frac{\tilde{p}_i}{\Omega_i}\right). \tag{3.37}$$

We can build up a closed expression for the change of basis connecting the operators x_i and p_i figuring in the original Hamiltonian, either in the Extended Basis or in the Localized Basis, to the second quantization operators $\hat{a}_i$ and $\hat{a}_i^\dagger$. We first invert formulas in equation (3.37):

$$\begin{cases} \tilde{x}_i = \frac{1}{\sqrt{2\Omega_i}}\left(\hat{a}_i + \hat{a}_i^\dagger\right), \\ \tilde{p}_i = \sqrt{\frac{\Omega_i}{2}}\frac{1}{i}\left(\hat{a}_i - \hat{a}_i^\dagger\right) \end{cases}. \tag{3.38}$$

We then invert (3.32) and plug the result of such an inversion into equation (3.38). In this way we obtain the desired change of basis for the Localized Basis:

$$\begin{cases} x_i = \sum_{j=1}^{2L} P_{ij}(\theta)\tilde{x}_j \\ p_i = \sum_{j=1}^{2L} P_{ij}(\theta)\tilde{p}_j \end{cases} \longrightarrow \begin{cases} x_i = \sum_{j=1}^{2L} \frac{1}{\sqrt{2\Omega_j}} P_{ij}(\theta)\left(\hat{a}_j + \hat{a}_j^\dagger\right) \\ p_i = \sum_{j=1}^{2L} \sqrt{\frac{\Omega_j}{2}}\frac{1}{i} P_{ij}(\theta)\left(\hat{a}_j - \hat{a}_j^\dagger\right) \end{cases}. \tag{3.39}$$

We finally rescale the masses and obtain the desired change of basis for the Extended Basis:

$$\begin{cases} x_i = \sum_{j=1}^{2L} \frac{1}{\sqrt{2m_i\Omega_j}} P_{ij}(\theta)\left(\hat{a}_j + \hat{a}_j^\dagger\right) \\ p_i = \sum_{j=1}^{2L} \sqrt{\frac{\Omega_j m_i}{2}}\frac{1}{i} P_{ij}(\theta)\left(\hat{a}_j - \hat{a}_j^\dagger\right) \end{cases}. \tag{3.40}$$

We conclude with the most general form for the relation linking q_i and p_i to $\hat{a}_i^\dagger$ and $\hat{a}_i$:

$$\begin{cases} x_i = \sum_{j=1}^{2L} \left[\frac{1}{\sqrt{m_i}}\right] \frac{1}{\sqrt{2\Omega_j}} \mathcal{D}_{ij}(\theta) \Phi_j^{hom}(i) \left(\hat{a}_j + \hat{a}_j^\dagger\right) \\ p_i = \sum_{j=1}^{2L} \left[\sqrt{m_i}\right] \sqrt{\frac{\Omega_j}{2}} \frac{1}{i} \mathcal{D}_{ij}(\theta) \Phi_j^{hom}(i) \left(\hat{a}_j - \hat{a}_j^\dagger\right) \end{cases}, \tag{3.41}$$

where the dependence on the defect strength θ is all contained in the masses m_i, which appear only in the case we use the Extended Basis, and in the matrix $\mathcal{D}_{ij}(\theta)$. We put into square brackets the multiplicative factor which should be added if we want to switch from the Localized Basis to the Extended Basis. This convention will be kept also in the subsequent sections.

3.4 Correlators and Covariance Matrix

General Form of Correlators We wish to build the 2-points correlator for positions and momenta, $\langle q_i q_j \rangle$ and $\langle p_i p_j \rangle$, which can be rewritten using the change of basis in equation (3.41):

$$\langle x_i x_j \rangle = \left[\frac{1}{\sqrt{m_i m_j}}\right] \sum_{n=1}^{2L} \sum_{m=1}^{2L} \sqrt{\frac{1}{2\Omega_n}} \sqrt{\frac{1}{2\Omega_m}} \mathcal{D}_{in}(\theta) \mathcal{D}_{jm}(\theta) \Phi_n^{hom}(i) \Phi_m^{hom}(j) \\ \langle 0 | \left(\hat{a}_n + \hat{a}_n^\dagger\right) \left(\hat{a}_m + \hat{a}_m^\dagger\right) | 0 \rangle, \tag{3.42}$$

$$\langle p_i p_j \rangle = \left[\sqrt{m_i m_j}\right] \sum_{n=1}^{2L} \sum_{m=1}^{2L} \sqrt{\frac{\Omega_n}{2}} \sqrt{\frac{\Omega_m}{2}} \mathcal{D}_{in}(\theta) \mathcal{D}_{jm}(\theta) \Phi_n^{hom}(i) \Phi_m^{hom}(j) \\ \left(\frac{1}{i}\right)^2 \langle 0 | \left(\hat{a}_n - \hat{a}_n^\dagger\right) \left(\hat{a}_m - \hat{a}_m^\dagger\right) | 0 \rangle . \tag{3.43}$$

Considering that:

$$\langle 0 | \left(\hat{a}_n + \hat{a}_n^\dagger\right) \left(\hat{a}_m + \hat{a}_m^\dagger\right) | 0 \rangle = \langle 0 | \hat{a}_n \hat{a}_m^\dagger | 0 \rangle = \delta_{nm}, \tag{3.44}$$

$$\left(\frac{1}{i}\right)^2 \langle 0 | \left(\hat{a}_n - \hat{a}_n^\dagger\right) \left(\hat{a}_m - \hat{a}_m^\dagger\right) | 0 \rangle = \langle 0 | \hat{a}_n \hat{a}_m^\dagger | 0 \rangle = \delta_{nm}, \tag{3.45}$$

we can further simplify expressions in equations (3.42) and (3.43):

$$\langle x_i x_j \rangle = \left[\frac{1}{\sqrt{m_i m_j}}\right] \sum_{n=1}^{2L} \frac{1}{2\Omega_n} \mathcal{D}_{in}(\theta) \mathcal{D}_{jn}(\theta) \Phi_n^{hom}(i) \Phi_n^{hom}(j), \tag{3.46}$$

$$\langle p_i p_j \rangle = \left[\sqrt{m_i m_j}\right] \sum_{n=1}^{2L} \frac{\Omega_n}{2} \mathcal{D}_{in}(\theta) \mathcal{D}_{jn}(\theta) \Phi_n^{hom}(i) \Phi_n^{hom}(j). \tag{3.47}$$

Some explicit calculations for the above correlators are contained in appendix A.

Covariance Matrix Then, our covariance matrix γ is the $4L \times 4L$ block diagonal matrix:

$$G = \left[\begin{array}{c|c} \mathcal{X} & \\ \hline & \mathcal{P} \end{array}\right], \tag{3.48}$$

where:

$$\mathcal{X} = \begin{bmatrix} x_{1,1} & \dots & x_{1,2L} \\ \vdots & \ddots & \vdots \\ x_{2L,1} & \dots & x_{2L,2L} \end{bmatrix}, \qquad \mathcal{P} = \begin{bmatrix} p_{1,1} & \dots & p_{1,2L} \\ \vdots & \ddots & \vdots \\ p_{2L,1} & \dots & p_{2L,2L} \end{bmatrix}. \tag{3.49}$$

We can rewrite the covariance matrix in this form:

$$G_T = \frac{1}{2}\left(P(\theta)\Omega^{-1}P(\theta) \oplus P(\theta)\Omega P(\theta)\right), \tag{3.50}$$

where $P(\theta)$ is defined by condition (3.34) and Ω is the diagonal matrix containing the spectrum of the Hamiltonian:

$$\Omega = diag(\Omega_1, \dots, \Omega_{2L}). \tag{3.51}$$

Linear Approximation for Covariance Matrix with Defect We want to study how the presence of a defect modifies the covariance matrix in absence of defect at first order in θ. We wish to obtain the matrix G_{lin} figuring in the first order Taylor expansion of the covariance matrix $G(\theta)$:

$$G(\theta) \simeq G_0 + \theta\, G_{lin} + O(\theta^2). \tag{3.52}$$

Then we plug the expansion in formula (3.52) into the expression (2.60) for $\mathcal{C}_2$ complexity. We obtain an expression for complexity at first order in θ, taking as reference state the no defect ground state and taking as target state the ground state of the defect chain with small θ:

$$\mathcal{C}_2 = \frac{\theta}{2\sqrt{2}} Tr\left[G_{lin} G_0^{-1}\right] + O(\theta^2). \tag{3.53}$$

Some explicit calculations for G_{lin} in the Localized Coordinates are contained in appendix A.

Large θ limit for the Covariance Matrix with Defect We wish to investigate the form that correlators in equations (3.46) and (3.47) assume in the limit where $\theta \to \infty$. We only analyze the case where Localized Coordinates are used, because, if we use Extended Coordinates we obtain some correlators

which are ill defined. Pictorially, using the Localized Basis, we obtain that the harmonic chain in the $\theta \to \infty$ is formed by two detached harmonic chains of length L with mass parameter Ω_0. To be more specific, we have that the matrix $\mathcal{D}_{ij}(\theta)$ assumes the following form:

$$\mathcal{D}_{ij}|_{\theta\to\infty} = \begin{cases} \sqrt{1+(-)^{j+1}} & i \in \{1,\dots,L\}, \\ \sqrt{1+(-)^{j}} & i \in \{L+1\dots 2L\}. \end{cases} \tag{3.54}$$

We can obtain the correlators in the limit $\theta \to \infty$ by simply plugging formula (3.54) into expressions for correlators in (3.46) and (3.47).

3.5 Complexity with Maximally Unentangled Reference State

In this section we want to show that $\mathcal{C}_2$ complexity is basically unaffected by the presence of the defect, if we take as reference the maximally unentangled state, which is the ground state of the Hamiltonian of decoupled oscillators in formula (2.25). The covariance matrix of this reference state is the tensor product of two matrices proportional to the identity:

$$G_R = \frac{1}{2\omega_0}\mathbb{1} \oplus \frac{\omega_0}{2}\mathbb{1}. \tag{3.55}$$

As a target state we choose the ground state of the Hamiltonian of the harmonic chain with defect in Localized Coordinates described in section 3.1, whose covariance matrix is given by expression (3.50). Hence, we can write down the relative covariance matrix Δ:

$$\begin{aligned} \Delta &= G_T G_R^{-1} \\ &= \left(\omega_0 P(\theta)\Omega^{-1}P(\theta)^T \oplus \frac{1}{\omega_0}P(\theta)\Omega P(\theta)^T\right), \end{aligned} \tag{3.56}$$

where $P(\theta)$ is the change of basis defined in equation (3.34) and Ω is the diagonal matrix containing the spectrum defined in equation (3.51). We notice that Δ enters into the formula (2.60) for $\mathcal{C}_2$ complexity of Gaussian states through the trace of the square its logarithm:

$$Tr\left(\log\Delta\right)^2 = Tr\left(\log\left[\omega_0 P(\theta)\Omega^{-1}P(\theta)^T \oplus \frac{1}{\omega_0}P(\theta)\Omega P(\theta)^T\right]\right)^2. \tag{3.57}$$

Then we can take the orthogonal change of basis $P(\theta) \oplus P(\theta)$ out of the matrix logarithm and exploit the invariance of the trace under orthogonal transformations:

$$Tr\left(\log\Delta\right)^2 = 2\sum_{i=1}^{2L}\left(\log\frac{\Omega_i}{\omega_0}\right)^2. \tag{3.58}$$

Then, we see that $\mathcal{C}_2$ complexity is independent of the defect parameter θ:

$$\mathcal{C}_2 = \frac{1}{2}\sqrt{\sum_{i=1}^{2L}\left(\log\frac{\Omega_i}{\omega_0}\right)^2}. \tag{3.59}$$

This is exactly the result in formula (2.37), obtained in [6] for the $\mathcal{C}_2$ complexity of the pure state of a harmonic chain without any defect. Hence, if we consider the maximally unentangled state as the reference state, we obtain that $\mathcal{C}_2$ does not feel the presence of the defect for any number of sites in the lattice.

4 Complexity for Harmonic Chain with Defect

In this section we study numerically the $\mathcal{C}_2$ complexity associated to the ground state of the harmonic chain with defect described in section 3. Our aim is to extract the divergence structure of $\mathcal{C}_2$ in the continuum limit.

4.1 Preliminaries

We make some preliminary considerations, which are useful to understand the results shown in the subsequent sections.

Target and Reference States We notice that the ground state of the harmonic chain with defect treated in section 3.1 is generally characterized by two different parameters:

$$|G.S.\rangle = |\Omega_0,\ \theta\rangle\,, \tag{4.1}$$

which are defined in the Hamiltonian given by expression (3.1). We choose as reference state the ground state with no defect ($\theta = 0$) and as target state the ground state with defect inserted ($\theta \neq 0$) and with the same mass parameter Ω_0. Then we find $\mathcal{C}_2$ complexity of quantum circuits connecting those two states:

$$\gamma\colon \left|\Omega_0,\ \theta^R = 0\right\rangle \longrightarrow \left|\Omega_0,\ \theta^T = \theta \neq 0\right\rangle \qquad \Omega_0 \in \mathbb{R},\ \theta \in \mathbb{R}. \tag{4.2}$$

This family of circuits corresponds to the red line in figure 6.

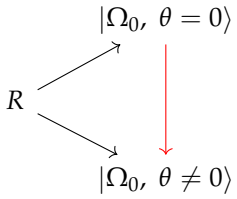

Figure 6: Quantum circuits connecting the chosen reference state R, and the gorund states of the harmonic chains with and without defect, $|\Omega_0,\ \theta = 0\rangle$ and $|\Omega_0,\ \theta\rangle$.

It should be stressed that this choice for the reference state is unusual, since in all the recent literature about complexity in quantum field theory the reference state is taken to be the maximally unentangled one, defined in section 2.2. If we followed the same path outlined in [6], we should have considered the $\mathcal{C}_2$ complexity of going from the chosen reference state R to the ground state of the harmonic chain with defect $|\Omega_0,\ \theta\rangle$ and eventually compare it to the complexity of going form the same reference state to the ground state of the same harmonic chain with no defect $|\Omega_0,\ \theta = 0\rangle$. The corresponding families

of circuits are represented by the black lines in figure 6. However, we have seen in section 3.5 that the choice of the maximally unentangled reference state implies that $\mathcal{C}_2$ complexity does not feel the presence of the defect. We will show instead, that the $\mathcal{C}_2$ complexity associated to the family of paths in formula (4.2) gives interesting results.

Continuum limit of a discrete lattice of harmonic oscillators In the following sections we will often mention the continuum or, equivalently, the quantum field theory limit of the harmonic lattice of oscillators. In this paragraph we briefly clarify the meaning of such an expression. Given the parameter Ω_0 we define the following dimensionless quantity: $2L\Omega_0$. For dimensional reasons, we assume that the quantum field theory limit is obtained increasing the number of sites $2L$ in our chain while keeping $2\Omega_0 L$ fixed. We point out that this limit is exactly the one studied in [62] to obtain the entanglement entropies. If $2\Omega_0 L \neq 0$, we have the massive quantum field theory, whereas, if $2\Omega_0 L = 0$ we obtain the massless or CFT limit. However, we cannot set sharply $2\Omega_0 L = 0$, i.e. $\Omega_0 = 0$, because of the presence of a zero mode in the eigenspectrum. Hence, we will consider the massless limit as that which is reached when $2\Omega_0 L$ is sufficiently small to make the curve that we are studying collapse when $2\Omega_0 L$ decreases further.

4.2 Numerical Results on the Segment

We study $\mathcal{C}_2$ complexity by means of formula (2.60) for the quantum circuit described in expression (4.2). We refer to the harmonic chain with defect defined on a segment described in section 3.1.

4.2.1 Localized Coordinates

We consider the Hamiltonian of our system in the Localized Coordinates as in formula (3.7) and therefore we use the correlators defined in equations (3.46) and (3.47) without the multiplicative factor in the square brackets.

Logarithmic Divergent Behavior We are interested at the divergence structure of $\mathcal{C}_2$ complexity in quantum field theory limit. In figure 7, we plot the dependence of $\mathcal{C}_2$ as a function of the logarithm of the total number of sites $Log(2L)$. First in figure 7a, we display results only for the case where $\theta = 1$, varying the parameter $2\Omega_0 L$ in the following range:

$$2\Omega_0 L \in \{10^{-6}, 10^{-4}, 10^{-2}, 1, 10^2\}. \tag{4.3}$$

Then, in figure 7b, we fix $2\Omega_0 L = 10^{-4}$ and vary the parameter θ in the following range:

$$\theta \in \{0.1, 0.5, 1.0, 5.0, 10.0\}. \tag{4.4}$$

We clearly see the presence of a logarithmic divergence structure in all the cases mentioned above. This is proved fitting the behaviour of $\mathcal{C}_2$ complexity with the following logarithmic model:

$$\mathcal{C}_2 \simeq \ a(\theta) \log(2L) + b(\theta) \qquad L \to \infty. \tag{4.5}$$

Results of this fit can be seen in figure 7 where the fit line perfectly overlaps the empty markers which represent the outcomes of our numerical computations. However, we have to observe that the coefficients $a(\theta)$ and $b(\theta)$ are not fixed if we perform the fit in different ranges of $2L$, but converge to an asymptotic value only in the quantum field theory limit defined in section 4.1. This is discussed in appendix B: we can say that the convergence of $a(\theta)$ and $b(\theta)$ to their asymptotic value in the continuum limit is almost reached for $2L$ as high as $2L > 1400$.

Coefficient of the Logarithmic Divergence We wish to study the dependence of the coefficient $a(\theta)$ in expression (4.5) on the defect parameter θ. Hence, we perform the logarithmic fit in the range

$$2L \in [1400, 1800], \tag{4.6}$$

where we are sure that the continuum limit is reached, and extract fit parameters for various values of θ. In figure 8, we plot $a(\theta)$ for several values of the adimensional parameter $2\Omega_0 L$ listed in (4.3). First, in figure 8a, we observe what happens varying θ within a range as wide as six orders of magnitude:

$$\theta \in [10^{-5}, 10], \tag{4.7}$$

and deduce that the growth of $a(\theta)$ is monotonic in θ and shows three regimes:

- Initial linear growth;
- Rapid transient between the the initial and the asymptotic regime;
- Final saturation.

The initial linear growth and the final saturation can be both obtained with an independent numerical method. In order to recover the initial linear growth, we use formula (3.53) to compute complexity at first order in θ in its quantum field theory limit. Then we perform a logarithmic fit with the model in formula (4.5) and extract the coefficient $a(\theta)$ at first order in θ. This coefficient is given by the dashed line in figure 8a. If instead, we want to obtain the saturation value of $\mathcal{C}_2$ we have to write correlators in the $\theta \to \infty$ limit using the prescription in formula (3.54) and then compute $\mathcal{C}_2$ in the quantum field theory limit. At this point, we perform a fit with the model in equation (4.5) and extract the saturation value of $a(\theta)$ for $\theta \to \infty$. This coefficient corresponds to the dashed

line in figure 8b. In this way we have realized two important self consistency checks, which, as it can be seen in figure 8, are fully satisfied.
Regarding the massless limit, we see that the curves for $a(\theta)$ clearly collapse in the limit where the dimensionless parameter $2\Omega_0 L$ is small only for $\theta \geq 10^{-2}$. Finally, looking at the plot in figure 8b, we see the coefficient $a(\theta)$ in the restricted range $\theta \in [0.1, 10.0]$, and notice that the massless limit is safely reached already for $2\Omega_0 L = 10^{-4}$ in such range of θ.

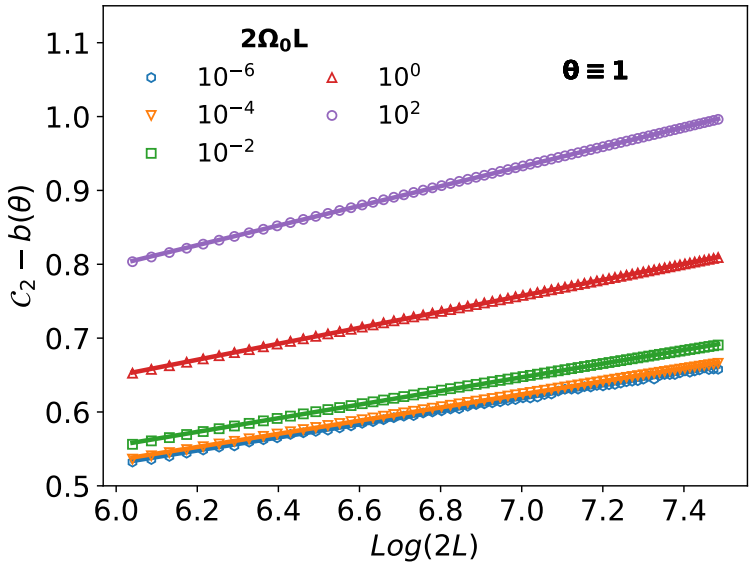

(a) *Logarithmic divergence at fixed* θ

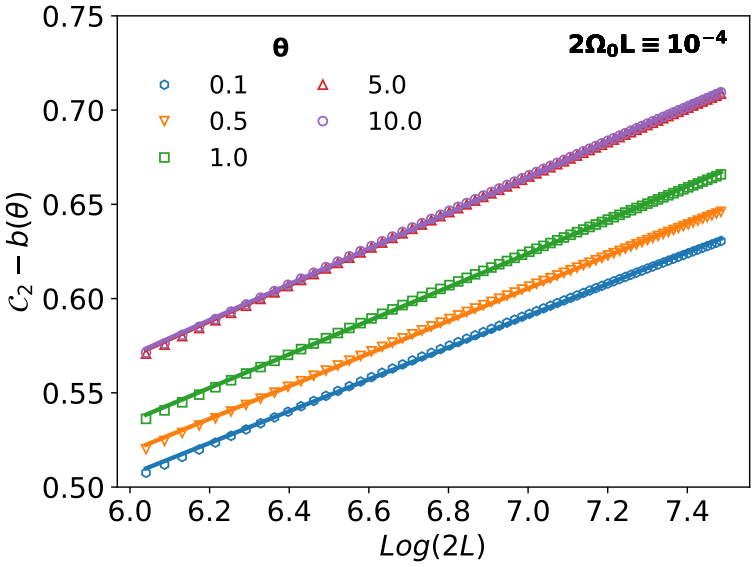

(b) *Logarithmic divergence at fixed* $2\Omega_0 L$

Figure 7: Logarithmic divergence of $\mathcal{C}_2$ complexity in Localized Coordinates in the continuum limit

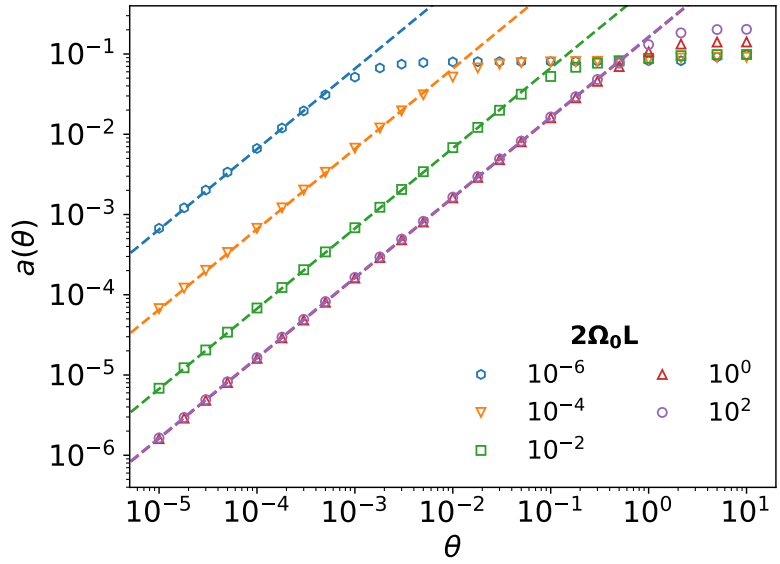

(a) $a(\theta)$

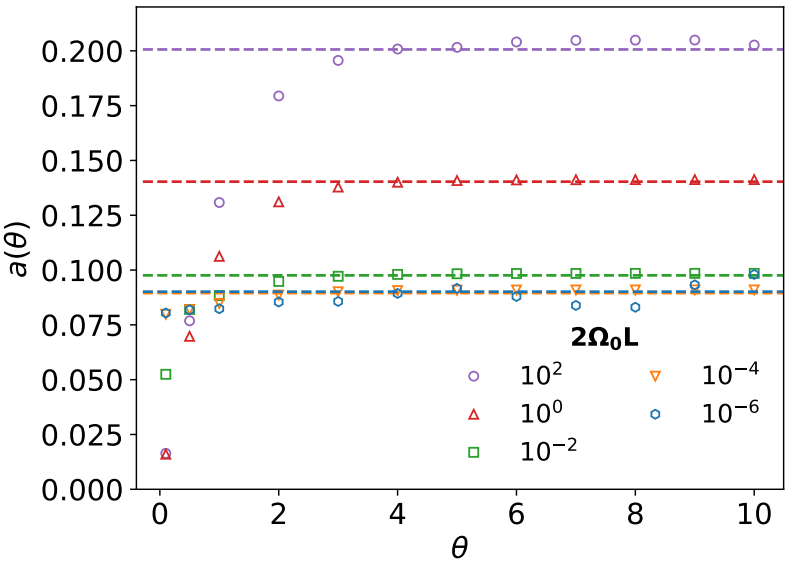

(b) $a(\theta)$- *Saturation Plot*

Figure 8: Coefficient $a(\theta)$ in formula (4.5) for various values of $2\Omega_0 L$.

4.2.2 Extended Coordinates

We consider the Hamiltonian of our system in the Extended Coordinates as in formula (3.1) and therefore we use the correlators defined in equations (3.46) and (3.47) including the multiplicative factor in square brackets.

Volumic Divergent Behavior We study again the divergence structure of $\mathcal{C}_2$ complexity in quantum field theory limit along the circuit in formula 4.2. In figure 9, we plot the the behavior of $\mathcal{C}_2$ as a function of the square root of the number of sites $\sqrt{2L}$, first keeping fixed $2\Omega_0 L$ and then keeping fixed θ. We clearly see the presence of a leading divergence proportional to $\sqrt{2L}$. To prove this, we perform a fit with the following model,

$$\mathcal{C}_2 \simeq d(\theta)\sqrt{2L} + e(\theta), \qquad 2L \to \infty \tag{4.8}$$

and see that the fit line perfectly crosses the empty markers in figure 9. Even in this case, the coefficients $d(\theta)$ and $e(\theta)$ reach their true value only asymptotically in the quantum field theory limit. Using methods analogous to those in appendix B, we checked that for $2L$ as high as 400 sites, the continuum limit is well reached.

Coefficient of the Volumic Divergence We choose a range of $2L$ where the quantum field theory limit is safely reached:

$$2L \in [400, 700], \tag{4.9}$$

and we study the behavior of the coefficient $d(\theta)$ in formula (4.8). We see that the coefficient $d(\theta)$ seems to have a linear increase in θ according to the following model:

$$d(\theta) \simeq \frac{1}{2}\theta + O(1). \tag{4.10}$$

This is perfectly visible in figure 10, where values of $d(\theta)$ perfectly fall on the line defined in equation (4.10).

Comparison with $\mathcal{C}_2$ in Localized Coordinates We have seen that even a simple and canonical change of coordinates as that in (3.6), modifies dramatically the divergence structure of $\mathcal{C}_2$ complexity. This is not surprising, given the basis dependence of complexity. To better understand this point, we can think of the meaning of modifying the parameter θ in the Localized and in the Extended Basis. If we consider the Hamiltonian in Extended Coordinates, as in formula (3.1), we see that a change in θ affects both the spring constant in the defect location and the masses $m_{1,2}$ of all the sites in the chain. This tells us that a quantum circuit like that in formula (4.2), which basically changes only θ, involves all the sites in the chain: therefore, it is expected that the

complexity associated to such circuit scales with a power law in the number of sites in the chain. Considering the infinite θ limit, we obtain this behavior of the parameters:

$$m_1 \to \infty \quad m_2 \to 0 \quad K_0 \to 0, \tag{4.11}$$

which corresponds to the situation where we have two detached chains whose respective Hamiltonians are ill defined. This is the reason why the coefficient $d(\theta)$ in figure 10 does not saturate for $\theta \to \infty$. If, instead, we consider the Hamiltonian in Localized Coordinate, as in formula (3.7), we see that varying θ corresponds simply to changing m_1 and m_2 in the two sites close in the defect locus and the spring constant between them. This makes us infer that the effect of the family of circuits in expression (4.2) is localized in the region near the defect locus. Hence, we do expect a divergence patter weaker than a power law for the corresponding $\mathcal{C}_2$ complexity: through our analysis we found that the UV divergence structure of $\mathcal{C}_2$ complexity is logarithmic. In the $\theta \to \infty$ limit, the situation that we obtain is very different: we have two detached chains, each with a well defined Hamiltonian of mass parameter Ω_0. For this reason the saturation of the coefficient $a(\theta)$ in figure 8 is perfectly expected.

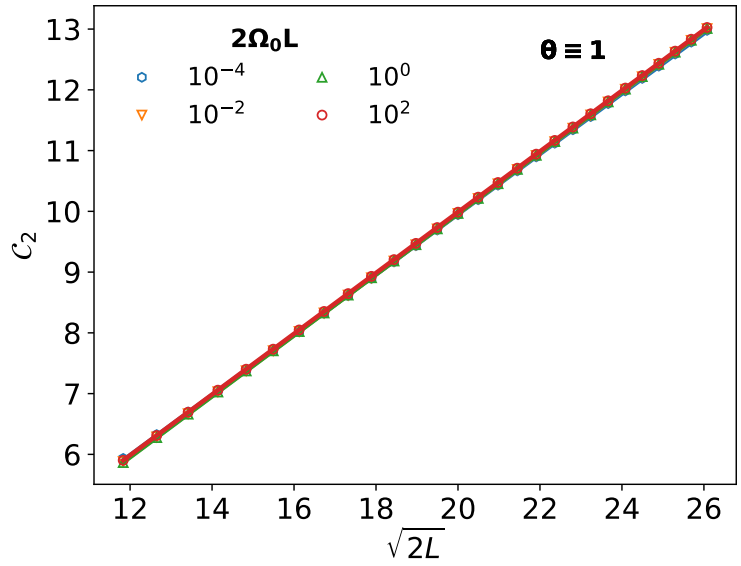

(a) *Volumic divergence at fixed* θ.

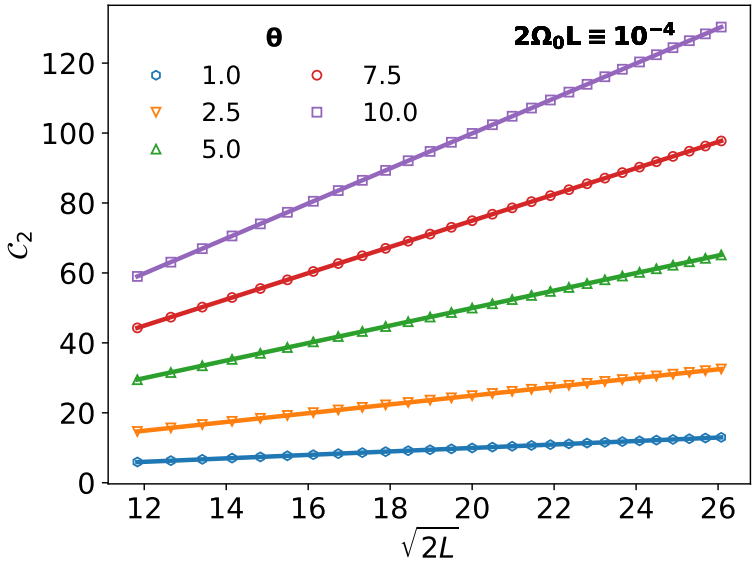

(b) *Volumic divergence at fixed* $2\Omega_0 L$.

Figure 9: Volumic divergence of $\mathcal{C}_2$ complexity in Extended Coordinates in continuum limit.

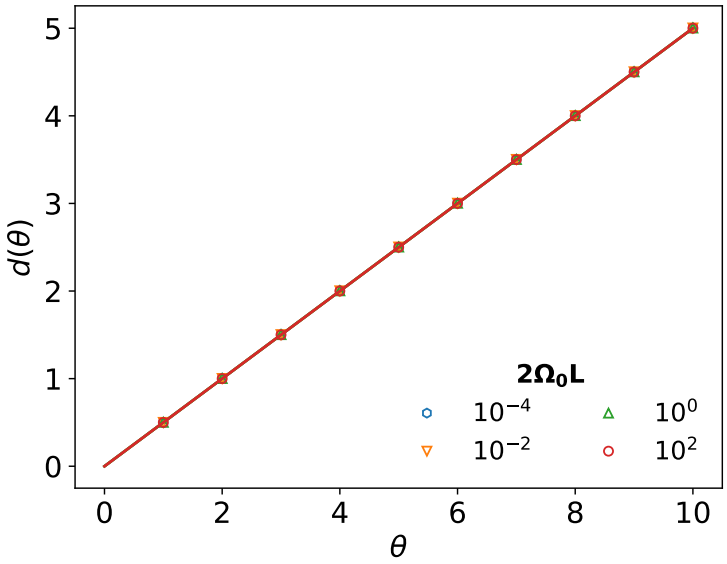

Figure 10: Coefficient $d(\theta)$ in formula (4.5) for various values of $2\Omega_0 L$.

4.3 Numerical Results on a Circle

Motivated by holography, we repeat the previous analysis in the case of the Hamiltonian of the harmonic chain with defect defined on a circle with two defect points. Such model is a straightforward extension of that in section 3 and is described in appendix C. We consider only Localized Coordinates, which are such that the Hamiltonian of our harmonic chain with defect on a circle is that in formula (C.2). By analogy with the previous case we find that the $\mathcal{C}_2$ complexity associated to the family of circuits in formula (4.2) displays the logarithmic divergence pattern depicted in formula (4.5). We report below the plot for the coefficient $a(\theta)$ and point out that it displays analogous features to the plot in figure 8a containing the coefficient $a(\theta)$ in the case of the harmonic chain with defect defined on a segment.

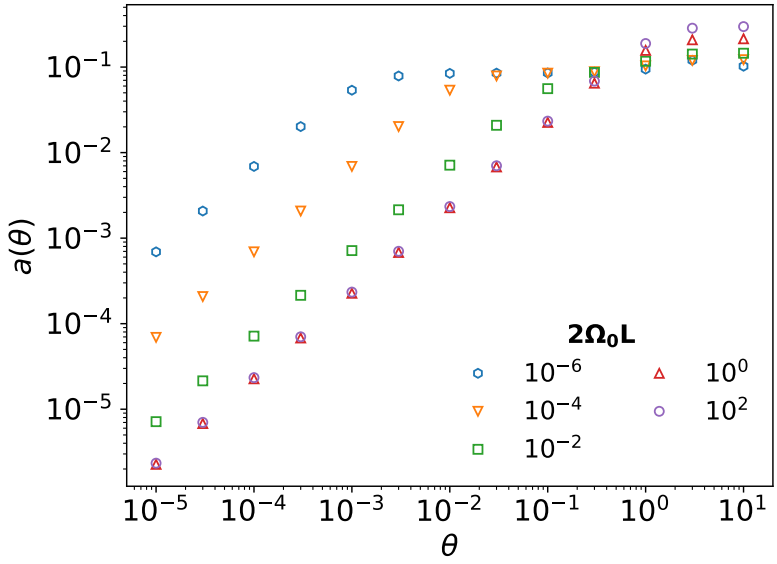

Figure 11: Coefficient $a(\theta)$ in formula (4.5). Ground state of the Hamiltonian in formula (C.2).

5 Entanglement across the Harmonic Chain with Defect

In this section we discuss the entanglement entropy for the half chain subregion of the harmonic chain with defect described in section 3.1. After briefly introducing the notion of entanglement entropy, we show that the entanglement entropy for the half chain subregion of the harmonic chain with defect has a logarithmic divergence pattern. We finally compare such divergence pattern with that of the $\mathcal{C}_2$ complexity in section 4.2.1.

5.1 Basics of Entanglement Entropy

Definition of Entangled State We consider a generic quantum mechanical theory defined on a bipartite Hilbert space:

$$\mathcal{H} = \mathcal{H}_A \otimes \mathcal{H}_B, \tag{5.1}$$

where we have that:

$$d = \dim \mathcal{H} \quad d_A = \dim \mathcal{H}_A \quad d_B = \dim \mathcal{H}_B. \tag{5.2}$$

We consider a pure state in the full Hilbert space:

$$|\psi\rangle \in \mathcal{H}, \tag{5.3}$$

and see that it admits a Schmidt decomposition in terms of the orthonormal bases of the two bipartite systems A and B [89–91]:

$$|\psi\rangle = \sum_{i}^{\min\{d_A, d_B\}} c_i \, |i\rangle_A \otimes |i\rangle_B \,, \tag{5.4}$$

where the orthonormal basis for the two subsystems are running over the same index $i \in \{1, \ldots, \min\{d_A, d_B\}\}$:

$$\{|i\rangle_A\} \subset \mathcal{H}_A, \quad \{|i\rangle_B\} \subset \mathcal{H}_B, \tag{5.5}$$

and the coefficients c_i can be taken to be:

$$c_i \in \mathbb{R}, \quad c_i \geq 0, \quad \sum_i |c_i|^2 = 1. \tag{5.6}$$

Under the conditions listed above, Schmidt decomposition is unique and the Schmidt rank is defined as the number of c_i which are non null. We define a pure state to be entangled if it has Schmidt rank strictly bigger than one, i.e. if it cannot be written as the tensor product of two pure states of the two subsystems A and B. We can generalize the definition of entanglement

including mixed states in the following way. Given a density matrix ρ acting on the elements of the full Hilbert space $\mathcal{H}$, we define the state to be entangled if it does not exist a decomposition of ρ in terms of the tensor product of two density matrices describing the quantum state of the two subsystems ρ_A and ρ_B [92]:

$$\rho = \rho_A \otimes \rho_B. \tag{5.7}$$

Entanglement Entropy for Pure State of a Bipartite System If we restrict to only pure bipartite states, the most used entanglement measure is the so called entanglement entropy. Suppose we have a pure state in a bipartite system:

$$\left|\psi\right\rangle \in \mathcal{H} = \mathcal{H}_A \otimes \mathcal{H}_B, \tag{5.8}$$

we take the reduced density matrix for the subsystem A as the trace of the full density matrix ρ over the subsystem B:

$$\rho_A = \underset{B}{Tr}\, \rho. \tag{5.9}$$

Then we define the entanglement entropy of the bipartite system as the Von Neumann entropy associated to one of the two subsystems [76,77]:

$$S_A(\rho) := -\underset{A}{Tr}\, \rho_A \log \rho_A. \tag{5.10}$$

Using Schmidt decomposition in equation (5.4), we can prove that that this definition, once the bipartition is given, does not depend on the specific subsystem on which we are tracing out:

$$S_A(\rho) = S_B(\rho). \tag{5.11}$$

In fact, we can obtain a simple expressions in terms of the coefficients of the Schmidt decomposition in formula (5.6):

$$S_A(\rho) = S_B(\rho) = -\sum_i c_i \log c_i. \tag{5.12}$$

Using this expression, we can see the entanglement entropy is null on a separable state and it attains its maximum when the Schmidt coefficients c_i are all equal, which is the maximally entangled state.
We finally revise some other important properties of the entanglement entropy. Suppose that we have a Hilbert space which is the union of three subspaces $\mathcal{H} = \mathcal{H}_A \cup \mathcal{H}_B \cup \mathcal{H}_C$, then the following inequalities hold:

- Positivity:
$$S_A \geq 0; \tag{5.13}$$
- Subadditivity [93,94] :
$$S_{A\cup B} \leq S_A + S_B; \tag{5.14}$$

- Strong Subadditivity [93, 94]:

$$S_{A\cup C} + S_{A\cap C} \leq S_A + S_B; \tag{5.15}$$

- Araki-Lieb Inequality [95]:

$$|S_A - S_B| \leq S_{A\cup B}. \tag{5.16}$$

Some measures of entanglement for the bipartition of a mixed state exist, but we do not discuss them here as this would be out of the scope of this thesis [96].

Entanglement Entropy for Gaussian States in a Finite Dimensional Hilbert Space We wish to calculate the entanglement entropy for a Gaussian state. We show that this is related uniquely to the symplectic spectrum of the corresponding covariance matrix, which is defined in formula (2.40) and uniquely characterizes the Gaussian state. With this aim we first revise some properties related to the fact the covariance matrix in expression (2.40) admits a Williamson decomposition [97]. Williamson theorem states that any real, symmetric and positive matrix with even size, such as the covariance matrix G, admits the following decomposition:

$$G = W^T \mathcal{D} W, \tag{5.17}$$

where:

- $W \in Sp(2N, \mathbb{R})$ is a symplectic matrix;
- $\mathcal{D} = diag(\sigma_1, \ldots \sigma_N) \oplus diag(\sigma_1, \ldots \sigma_N)$ is the diagonal matrix containing the symplectic eigenvalues and is uniquely determined up to permutations of the symplectic eigenvalues.

A practical way to find computationally the symplectic eigenvalues consists in the diagonalization of the matrix M defined as follows:

$$M := G\, J, \tag{5.18}$$

where J is the $2N \times 2N$ symplectic unit and G is the covariance matrix. The spectrum of M yields directly the symplectic eigenvalues:

$$Spectrum(M) = \{\pm i\sigma_1, \ldots, \pm i\sigma_N\}. \tag{5.19}$$

It has been shown in [19] and [98] that the validity of the uncertainty principle implies the following condition on the covariance matrix G:

$$G + \frac{i}{2} J \geq 0, \tag{5.20}$$

where J is the symplectic unit. The authors of [19] showed that combining this condition with the Williamson decomposition, a constraint on the symplectic eigenvalues can be derived:

$$\sigma_i \geq \frac{1}{2}, \tag{5.21}$$

where in the case of the pure state:

$$\sigma_i = \frac{1}{2} \qquad \forall i \in \{1, \ldots, N\}. \tag{5.22}$$

Now, we are ready to briefly review the calculation of the entanglement entropy for the Gaussian states of a finite dimensional Hilbert space, following reference [99]. We focus on a chain of N coupled quantum harmonic oscillators with Hamiltonian in formula (3.33), where the Hilbert space $\mathcal{H}$ is the tensor product of N single-oscillator Hilbert spaces:

$$\mathcal{H} = \bigotimes_{i=1}^{N} \mathcal{H}_i. \tag{5.23}$$

The ground state of such system is a Gaussian state as defined in formula (2.38) and is completely characterized by its covariance matrix G written in expression (2.40). We choose a subsystem made of $N_{sub} \leq N$ harmonic oscillators, whose Hilbert space is given by:

$$\mathcal{H}_{sub} = \bigotimes_{i=1}^{N_{sub}} \mathcal{H}_i, \tag{5.24}$$

and whose covariance matrix γ_{sub} is simply obtained tracing out the remaining subsystem on the full covariance matrix G:

$$G_{sub} = \underset{\mathcal{H}/\mathcal{H}_{sub}}{Tr} G. \tag{5.25}$$

At this point we recall the existence of a prescription for the entanglement entropy associated to this bipartition [100], showing that it depends uniquely on the symplectic eigenvalues $\{\sigma_i\}_{i=1,\ldots,N_{sub}}$ of the subsystem covariance matrix G_{sub} :

$$S = \sum_{i=1}^{N_{sub}} \left[\left(\sigma_i + \frac{1}{2}\right) \log\left(\sigma_i + \frac{1}{2}\right) - \left(\sigma_i - \frac{1}{2}\right) \log\left(\sigma_i - \frac{1}{2}\right) \right]. \tag{5.26}$$

A derivation of formula (5.26) is fully given in [99] and is not reported in this thesis.

5.2 Entanglement Entropy for the Half Harmonic Chain with Defect

In this section, we compute the entanglement entropy associated to the half chain subregion in the harmonic chain with defect in formula (3.7). We focus on the bipartition where the chain of length $2L$ in figure 4 is divided into two perfect halves by the locus of the defect.

Continuum Limit of the Entanglement Entropy for a Critical Harmonic Chain with Defect Focusing on the harmonic chain with defect in formula (3.1) and choosing the bipartition specified above, an exact result for the entanglement entropy in the massless continuum limit has been obtained in [62]. This result is the same as that previously derived in a defect conformal field theory framework in [83]. It has been shown that the entanglement entropy in massless continuum limit displays a leading logarithmic divergence:

$$S = \frac{c_{eff}(\theta)}{6} \log L + \dots \qquad L \to \infty, \quad \Omega_0 L = 0, \tag{5.27}$$

with a coefficient $c_{eff}(\theta)$ which has a complicate dependence on the defect parameter θ:

$$c_{eff}\left(s = \frac{1}{\cosh\theta}\right) = \frac{3}{2}s + \frac{3}{\pi^2}\{\left[(1+s)\ln(1+s) + (1-s)\ln(1-s)\right]\ln s + \\ + \left[(1+s)Li_2(-s) + (1-s)Li_2(s)\right]\}. \tag{5.28}$$

In the no defect limit $\theta \to 0$, we notice that the result is in agreement to what was theoretically derived in [78–81] for the entanglement entropy in a conformal field theory in 1+1 dimensions:

- The leading divergence is logarithmic;
- The coefficient $c_{eff}(\theta)$ gives back the unit central charge of the free boson conformal field theory in the limit where the defect is absent:

$$\lim_{\theta \to 0} c_{eff}(\theta) = 1. \tag{5.29}$$

For this reason we regard the function $c_{eff}(\theta)$ as an *effective central charge* telling us that the effect of the presence of the defect is to somehow decrease the central charge that the entanglement entropy feels in the massless quantum field theory limit. A plot of such exact result for $c_{eff}(\theta)$ is the continuous line in figure 12.

Numerical Results for Entanglement Entropy of Half Critical Harmonic Chain with Defect We compute numerically the entanglement entropy for half of the harmonic chain with defect applying formula (5.26) for the entanglement entropy of Gaussian states and following the procedure outlined in section 5.1. We study the entanglement entropy in the continuum limit defined in section 4.1, by increasing the number of sites in the chain $2L$ while keeping the parameter $2\Omega_0 L$ fixed to the values listed below:

$$2\Omega_0 L \in \{10^{-6}, 10^{-4}, 10^{-2}, 1, 10^2\}, \tag{5.30}$$

and iterate the procedure for various values of $\theta \in [0, 10]$. We clearly observe that in all cases the entanglement entropy diverges logarithmically in the continuum limit:

$$S = \frac{c(\theta)}{6} \log L + \dots \qquad L \to \infty, \quad \Omega_0 L \neq 0. \tag{5.31}$$

At this point we perform the logarithmic fit and compute numerically the coefficient $c(\theta)$. We choose the range of $2L$ where we perform the fit:

$$2L \in [2600, 3000], \tag{5.32}$$

in such a way that the number of sites is sufficiently high to ensure the convergence of the entropy to its quantum field theory limit. We verified such convergence with analogous methods to those used in appendix B for $\mathcal{C}_2$ complexity. We observe that in the limit $2\Omega_0 L \to 0$, we should expect that curve for $c(\theta)$ collapses on the curve $c_{eff}(\theta)$ in formula (5.28). However, in figure 12, we see the comparison between our numerical computations for $c(\theta)$ and $c_{eff}(\theta)$. We notice that $c(\theta)$ effectively collapses on $c_{eff}(\theta)$ in the limit $2\Omega_0 L \to 0$ only in the range:

$$\theta \in [0, 1]. \tag{5.33}$$

For $\theta > 1.0$, the numerical extrapolation of the coefficient $c(\theta)$, not only lies far from $c_{eff}(\theta)$ but does not even seem to converge to that behavior in the limit $2\Omega_0 L \to 0$. This is partly expected because in [62] it has been shown that only for θ sufficiently small numerical estimates for $c_{eff}(\theta)$ reach easily the exact curve and it is explicitly said that for higher values of θ, we cannot observe any agreement between theoretical calculations and numerical computations. This might be a sign of the fact that our theoretical model breaks for big values θ or it can be related to the fact that strictly speaking we are not taking the *massless* quantum field theory limit. In fact, we cannot set sharply $2\Omega_0 L = 0$, because of the presence of a zero mode in the spectrum of the defect harmonic chain (formula (C.5)); instead, we have to take sufficiently small values of $2\Omega_0 L$. Practically we assume that the massless limit is reached when the curves for $c(\theta)$ coincide when we lower further the value of $2\Omega_0 L$. In our case, we see in figure 12b that when $2\Omega_0 L = 10^{-4}$, the massless quantum field theory

limit is reached only for $\theta < 3$. This makes us believe that the mismatch between exact results and numerical computation is not due to impossibility of imposing rigorously the massless limit.

Comparison between the coefficients $c(\theta)$ and $a(\theta)$ We want to understand if some relation exists between $a(\theta)$ and $c(\theta)$, i.e. between the logarithmic divergence pattern of $\mathcal{C}_2$ complexity and of the entanglement entropy S. We first notice that in the no defect limit the two coefficients $a(\theta)$ and $c(\theta)$ have a different behavior:

$$c(\theta = 0) = 1 \qquad a(\theta = 0) = 0. \tag{5.34}$$

This observation leads us to plot $1 - c(\theta)$ and compare this to the plot of $a(\theta)$ in figure 13. Keeping in mind also the plots in figure 8 and 12, we notice that some crucial differences are present between $a(\theta)$ and $1 - c(\theta)$:

- The small θ behavior is linear for $a(\theta)$, whereas it is parabolic for $1 - c(\theta)$.
- The coefficient $a(\theta)$ saturates to different values if we change $2\Omega_0 L$, whereas $1 - c(\theta)$ saturates to the same constant value even if we change $2\Omega_0 L$.
- In the numerical computations for $1 - c(\theta)$ we see that for $2\Omega_0 L = 10^{-4}$ a step like behavior appears The initial increase in $1 - c(\theta)$ at small θ is then followed by a plateaux, followed by another increase up to the final saturation. Such behavior is not observed in $a(\theta)$.

Those substantial differences lead us to conclude that there is no simple relation between $a(\theta)$ and $1 - c(\theta)$.

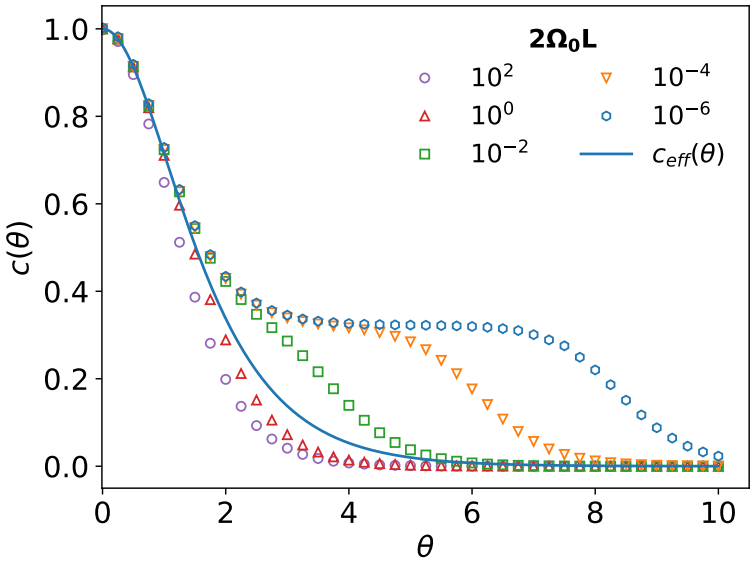

(a) $\theta \in [0, 10.0]$

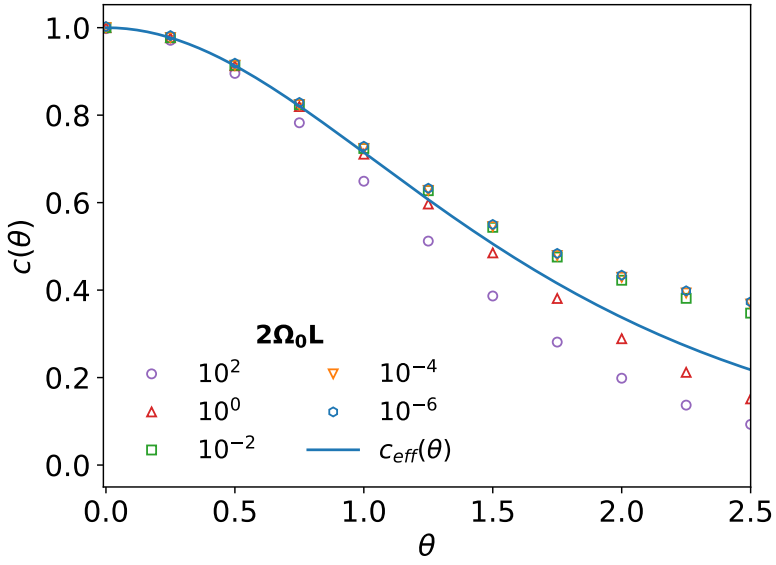

(b) $\theta \in [0, 2.5]$

Figure 12: Coefficient $c(\theta)$ in (5.31)
and the effective central charge $c_{eff}(\theta)$ in (5.27).

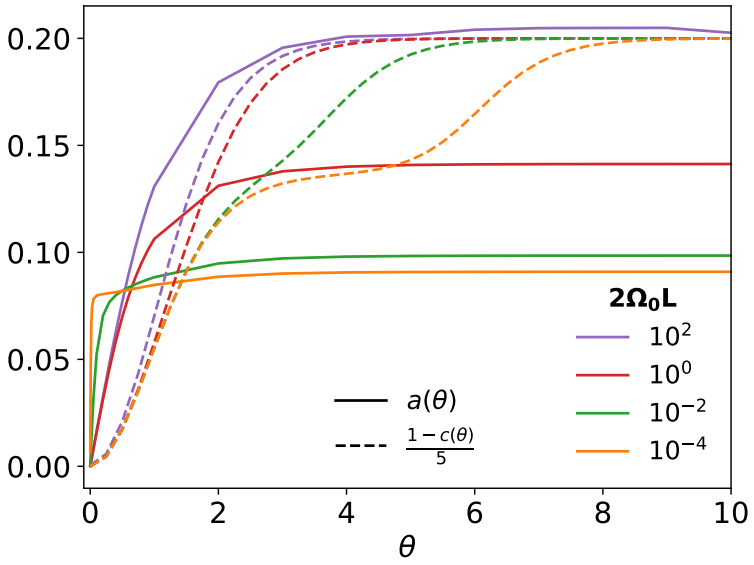

Figure 13: Comparison between $(1 - c(\theta))$ and $a(\theta)$. Lines are obtained joining the dots from our numerical computations. $(1 - c(\theta))$ has been rescaled for graphical reasons.

6 Holographic Complexity in Presence of Defect

In this section we summarize the calculations made in [75], for holographic complexity in presence of defect. Then, we try to explain how those results are related to those we found in section 4.

6.1 Symmetric Defect in AdS_3

The three dimensional toy model which was used in [75] to describe a symmetric defect in AdS_3 had been previously introduced in [101]. Let us consider a three dimensional solution of Einstein equations with negative cosmological constant and add to it a two dimensional brane. The action of the model reads:

$$S = \frac{1}{16\pi G_N}\int d^3x\sqrt{-g}\left(R+\frac{2}{L^2}\right) - \lambda\int_{defect\ locus} d^2x\sqrt{-g_{IND}},$$

where λ is the brane tension, L is AdS_3 radius, R is Ricci scalar and g_{IND} is the induced metric on the defect locus. In order to find a solution, we can plug this ansatz into Einstein equations:

$$ds^2 = L^2(dy^2 + e^{2A(y)}ds^2_{AdS_2}),$$

with

$$ds^2_{AdS_2} = dr^2 - \cosh r^2\ dt^2,$$

and impose the following requirements:

- the defect is located on a thin AdS_2 brane at y = 0;
- pure AdS_3 is recovered in the limit $\lambda \to 0$, which concretely implies the following condition:

$$e^{2A(y)} \xrightarrow[\lambda\to 0]{} \cosh^2 y. \tag{6.1}$$

It has been shown in [101] that the solution for $A(y)$ is given by:

$$e^{A(y)} = \cosh\left(|y| - y^*\right) \tag{6.2}$$

where y^* is defined through the relation:

$$\tanh y^* = 4\pi G_N \lambda L, \tag{6.3}$$

which gives the condition:

$$\lambda \ \leq\ \frac{1}{4\pi G_N L}. \tag{6.4}$$

Then the geometry of the model, represented in figure 14, is described by the following metric:

$$ds^2 = L^2\left[d\bar{y}^2 + \cosh\left(|\bar{y}| - y^*\right)^2\left(-\cosh^2 r dt^2 + dr^2\right)\right]. \tag{6.5}$$

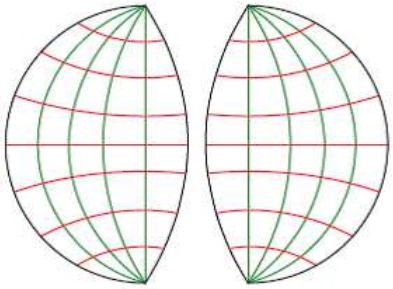

Figure 14: Geometry of defect AdS_3. Figure taken form [75].

We can see that fixing the coordinate y, we get AdS_2 slices, which are represented by green lines in figure 14; in particular fixing $y = \pm y^*$ we obtain the defect region. Hence, it is possible to obtain two patches, which are spanned by the ranges of coordinate $y \in [-\infty, y^*]$ and $y \in [-y^*, \infty]$ and are glued together at the defect location $y = \pm y^*$. In figure 14, red lines instead represent r constant curves, which are geodesics of the model and are orthogonal to y constant lines. Boundary is located at both $y = \pm\infty$ and $r = 0, \pm\infty$. The metric in equation (6.5) can be reshuffled in a simpler form, performing this shift:

$$\begin{cases} \bar{y} \to y + y^*, \ y < 0 \\ \bar{y} \to y - y^*, \ y > 0 \end{cases}, \tag{6.6}$$

and obtaining:

$$ds^2 = L^2 \left[dy^2 + \cosh^2 y \left(-\cosh^2 r dt^2 + dr^2 \right) \right]. \tag{6.7}$$

Another useful form for the metric in expression (6.7), is obtained through the following change of coordinates:

$$\begin{cases} \tanh r = \sin\phi \cos\theta \\ \sinh y = \tan\phi \sin\theta \end{cases}, \tag{6.8}$$

which gives the following metric:

$$ds^2 = \frac{L^2}{\cos^2\phi}(-dt^2 + d\phi^2 + \sin^2\phi d\theta^2), \qquad \phi \in \left[0, \frac{\pi}{2}\right] \ \theta \in \mathbb{R}, t \in \mathbb{R}. \tag{6.9}$$

In this case we can regard the constant time slice as a Poincaré disk with radial coordinate $\phi \in \left[0, \frac{\pi}{2}\right]$. Finally, we rescale t to introduce a new scale, which sets the curvature of boundary:

$$\tau = L_B t. \tag{6.10}$$

6.2 Results for Complexity equals Volume

In this subsection, we summarize the calculations which were performed in [75] to calculate holographic complexity for the conjecture *complexity equals volume* in the peculiar set up of symmetric defect AdS_3. We first discuss briefly how the authors of [75] regularized the theory and then we outline their results for complexity.

Cutoff Regularization Since holographic complexity is expected to be divergent, there is the need to choose a regularization scheme for the model we are considering. The authors of [75] decide to use cutoff regularization. For this reason they first bring the metric in equation (6.9) into the holographic form:

$$ds^2 = \frac{L^2}{z^2}\left(dz^2 + g_{ij}(x,z)dx^i dx^j\right), \tag{6.11}$$

using this change of variable:

$$z = 2L_B \frac{\cos\phi/2 - \sin\phi/2}{\cos\phi/2 + \sin\phi/2}. \tag{6.12}$$

Then, they adopt the usual holographic cutoff, the Fefferman-Graham cutoff:

$$z = \delta, \tag{6.13}$$

and translate it into the coordinate systems specified in expressions (6.7) and in (6.9):

$$\phi = \frac{\pi}{2} - \hat{\delta}, \qquad \cosh y \cosh r = \frac{1}{\sin\hat{\delta}}, \tag{6.14}$$

where they introduce the dimensionless cutoff:

$$\hat{\delta} = \frac{\delta}{L_B}. \tag{6.15}$$

However, such choice for the cutoff gives a non smooth surface on the defect locus. This is sketched in figure 15, where one of the two time constant patches of defect AdS_3 is shown and the standard Fefferman-Graham cutoff surface corresponds to the dashed blue line, which is not orthogonal to the locus of the defect. The solution to this problem consists in considering a different cutoff surface in the region near the defect and then glue it smoothly to the standard cutoff cutoff surface used in the region away from the defect. The near defect cutoff surface is chosen as follows:

$$\tanh r = \sin\phi\cos\theta = \cos\hat{\delta}, \tag{6.16}$$

and is such that, in (τ, y, r) coordinate it follows r constant lines that are orthogonal to y constant surfaces and consequently to the locus of the defect $y = \pm y^*$. The cutoff surfaces described in expressions (6.14) and (6.16), smoothly interpolate at $y = 0$. This is again sketched in figure 15, where the near defect cutoff is given by the red line and the $y = 0$ locus is the vertical black line.

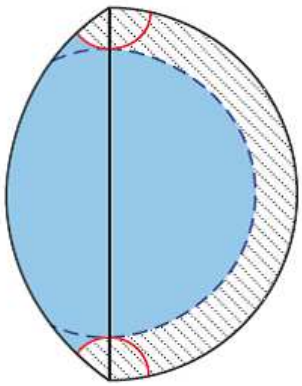

Figure 15: Fefferman-Graham cutoff surface. Figure taken from [75].

Complexity for the Pure State According to formula (2.61), holographic complexity for the $\mathcal{CV}$ conjecture in this spacetime model, is proportional to the volume of the constant time slice of defect AdS_3. In figure 16, we can see one patch of the time $\tau = 0$ slice of defect AdS_3, where the volume to be integrated is divided in two parts:

- the region near defect V_1, where we integrate the volume element using (y, r) coordinates:

$$V_1 = 2L^2 \int_{-y*}^{0} \cosh y \int_0^{\tanh^{-1}\cos\hat{\delta}} dr; \tag{6.17}$$

- the region away from defect V_2, where we integrate the volume element using (ϕ, θ) coordinates:

$$V_2 = L^2 \int_0^{\pi} d\theta \int_0^{\frac{\pi}{2}-\hat{\delta}} d\phi \frac{\sin\phi}{\cos^2\phi}. \tag{6.18}$$

In this way, the authors of [75] obtain holographic complexity for the $\mathcal{CV}$ conjecture:

$$\begin{aligned} \mathcal{C}_V &= \frac{2}{G_N L}(V_1 + V_2) \\ &= \frac{4c_T}{3}\left(\frac{\pi}{\hat{\delta}} + 2\sinh y^* \ln\frac{2}{\hat{\delta}} - \pi\right), \end{aligned} \tag{6.19}$$

where y^* is the parameter defined in formula (6.3) and c_T is the Brown-Henneaux central charge in [102], given by:

$$c_T = \frac{3L}{2G_N}. \tag{6.20}$$

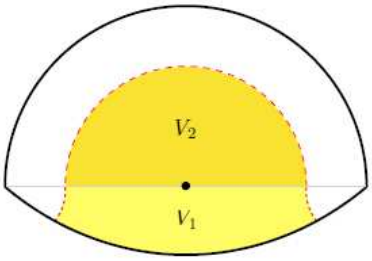

Figure 16: Integration Region for $\mathcal{CV}$ conjecture. Figure taken from [75].

We clearly see that the presence of the defect gives a subleading logarithmic divergence, which is contained in the boxed part of formula (6.19).

6.3 Results for Complexity equals Action

In this subsection, we summarize the calculations which were performed in [75] to obtain holographic complexity for the conjecture *complexity equals action* in the peculiar set up of symmetric defect AdS_3. We first discuss briefly the structure of the Wheeler-DeWitt patch and then we will outline the results for complexity in the case of both the pure and mixed state.

Structure of the Wheeler-DeWitt patch The Wheeler-DeWitt (WDW) patch is defined as the union of all spacelike surfaces anchored at the boundary time slice where the state is defined. In order to find it, the procedure used in [75] is to throw null geodesics starting from the boundary of $t = 0$ time slice and then identify the boundary of WDW patch. In figure 17, we see the structure of the future half of the WDW patch if the boundary state is defined at time $t = 0$. In the region away from defect, the WDW patch is limited by the geodesics starting from the points on the pieces of boundary $y = \pm\infty$: it takes the form of a portion of cone, i.e. the blue surface in figure 17. On the other hand, in the region near the defect, the structure of WDW patch is modified by the presence of the two points in the intersection between the defect locus and the boundary, i.e. at $r = 0, \pm\infty$. The equations which describe null geodesics starting from those two points are:

$$\tanh r = \cos t \quad y \equiv y_0, \tag{6.21}$$

In figure 17, the WDW patch near defect is limited by the green surfaces, whereas the yellow ones correspond to the defect location where the two pieces of WDW patch are glued together.

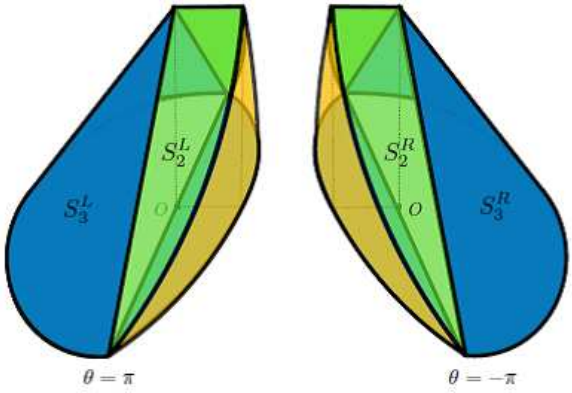

Figure 17: Wheeler-DeWitt patch in defect AdS_3. Figure taken from [75].

Complexity for the Pure State According to formula (2.66), the authors of [75] calculate holographic complexity as the gravitational action evaluated on the WDW patch depicted in figure 17 following the prescriptions described in section 2.3. Their result for holographic complexity of the pure state is given by the following expression:

$$\mathcal{C}_A = \frac{c_T}{3\pi}\left[\frac{1}{\hat{\delta}}\left(\ln\frac{l_{ct}}{L}+1\right)+\frac{\pi}{2}\right], \tag{6.22}$$

where c_T is the Brown-Henneaux central charge, l_{ct} is a counterterm scale introduced in I_{CT} piece in expression (2.67) for the gravitational action and L is AdS radius. Expression (6.22) basically tells us that complexity for $\mathcal{CA}$ conjecture does not feel the presence of the defect. We should point out that in [75], subleading logarithmic divergences showing a defect dependence appear when calculating the single terms in equation (2.67); however, their effect disappears when we sum up those terms to obtain the total gravitational action on the WDW patch.

6.4 Comparison with $\mathcal{C}_2$ Complexity

In this subsection we try to understand if there is some relationship between the holographic problem studied in [75] and the problem we discussed in section 4.

Summary of the Results in [75] We here summarize the results previously discussed for holographic complexity in a set up with defect. We consider the

quantity that in [75] is called *complexity of formation of the defect*:

$$\Delta\mathcal{C}^{QFT} = \mathcal{C}^{QFT}_{R\to T_{defect}} - \mathcal{C}^{QFT}_{R\to T_{no\ defect}}, \tag{6.23}$$

where T and R are the target and reference state defined in the dual quantum field theory living on the boundary of the symmetric defect AdS_3 space described in section 6.1. If the nature of the reference state R still remains an open problem in holography, the target state is known to be the ground state of the dual quantum field theory. Hence, making the identification

$$\mathcal{C}^{holo} \longleftrightarrow \mathcal{C}^{QFT}_{R\to T}, \tag{6.24}$$

we rewrite the results of sections 6.2 and 6.3 in terms of the complexity of formation of the defect. For the pure state we have that the two conjectures $\mathcal{CV}$ and $\mathcal{CA}$ give:

$$\Delta\mathcal{C}_V = \frac{8c_T}{3}\sinh y^* \ln\frac{2}{\tilde{\delta}}, \tag{6.25}$$

$$\Delta\mathcal{C}_A = 0. \tag{6.26}$$

We finally remember that y^* is related to the tension of the defect brane λ through equation (6.3).

Search for the Dual Quantum Field Theory Set Up At the moment, it is not known how to calculate complexity for an interacting quantum field theory. Hence, the best that we can do is to calculate complexity for a free field theory which mimics the features of the dual field theory of the defect AdS_3 space described in section 6.1. The requirements we ask on such free field theory are those:

- The theory should be defined on a circle;
- The theory should contain two defect points at diametrically opposite locations on the circle;
- The defect should be of the type described in [63].

It is evident that the first two conditions are not satisfied by the quantum field theory limit of the harmonic chain considered in section 3. However, as specified in [62], such a harmonic chain contains in its conformal field theory limit a defect of the type described in [63]. Hence, we could try to write a harmonic chain with analogous features to the one we described in section 3.1 but defined on a circle and containing two defect points. This is done in appendix C, where it is also shown that we can diagonalize the Hamiltonian on a circle with two defect points using almost the same techniques of section 3.2. At this point, we can calculate $\mathcal{C}_2$ complexity using this straightforward extension of

the set up in section 3. We choose the Localized Coordinates, because the holographic defect in section 6.1 is localized in two points of the boundary. Finally we have to find a dictionary connecting the quantities figuring in expression (6.26) for holographic complexity and the quantities that we used in section 4 to study the lattice problem. We have that in holography divergences are expressed in terms of the inverse of Fefferman-Graham cutoff $\frac{1}{\hat{\delta}}$, whereas in lattice field theory we express divergences in terms of the total number of sites, which is $4L$ in the case of the harmonic chain defined on a circle. Considering that through the holographic correspondence, the Fefferman-Graham cutoff corresponds to an ultraviolet cutoff in the dual quantum field theory, we can put forward the following identification:

$$\frac{1}{\hat{\delta}}|_{holography} \longleftrightarrow 4L|_{lattice}. \tag{6.27}$$

Quantum Field Theory Complexity with Generic Reference State At the moment, the best proposal for the reference state of holography is the maximally unentangled reference state, which is the ground state of the Hamiltonian of decoupled oscillators in formula (2.25). If we consider the maximally unentangled state as the reference state, we obtain that $\mathcal{C}_2$ does not feel the presence of the defect for any number of sites in the lattice. Therefore, we obtain that in the quantum field theory limit the complexity of formation of the defect, if the reference state is the maximally unentangled one, is:

$$\Delta\mathcal{C}_2 = 0. \tag{6.28}$$

This seems to support the holographic result coming form the $\mathcal{CA}$ conjecture. However, there is still no clear agreement on the nature of the reference state, therefore we will try to extract some information about the dual of the holographic complexity of formation of the defect in a way that is independent from the reference state. As it was done in the previous paragraph, we will mimic the dual field theory with the continuum limit of the harmonic chain in Localized Coordinates defined on a circle with two defect points, which is described in appendix C. In sections 4.3, we computed the $\mathcal{C}_2$ complexity of moving from the ground state of a homogeneous harmonic chain on a circle to that of a harmonic chain on a circle with two defect points inserted:

$$\mathcal{C}_{2\ T_{no\ defect}\to T_{defect}}, \tag{6.29}$$

which is associated to the path represented by the red line in figure 6. On the other hand, if we want to calculate the complexity of formation of the defect $\Delta\mathcal{C}_2$, we need the following quantities:

$$\mathcal{C}_{2\ R\to T_{defect}}, \quad \mathcal{C}_{2\ R\to T_{no\ defect}}, \tag{6.30}$$

which are associated to the black lines in figure 6 and are impossible to compute if we do not know the nature of the reference state R. However, we can

see that the quantities in expression (6.29) and (6.30) can be related by means of the triangular inequality:

$$\Delta\mathcal{C}_2 = \mathcal{C}_{2\ R\to T_{defect}} - \mathcal{C}_{2\ R\to T_{no\ defect}} \leq \mathcal{C}_{2\ T_{no\ defect}\to T_{defect}}. \tag{6.31}$$

This tells us that studying the quantity defined in formula (6.29) we obtain an upper bound on the complexity of formation of the defect in a free field theory. We can use the result derived in section 4.3 to say that such upper bound on the complexity of formation of the defect has a logarithmic divergence pattern. The coefficient $a(\theta)$ of the logarithmic divergence is that contained in figure 11. It should be pointed out that those results are valid only for the pure state case.

7 Conclusions

In this thesis, we reviewed the notion of complexity of Gaussian states in a lattice quantum field theory framework, and applied some of the tools present in literature to the case of the harmonic chain with defect in [62].

We used a specific kind of complexity, namely $\mathcal{C}_2$ complexity, associated to the choice of the F_2 cost function. Such choice is due to the fact that F_2 cost function induces the structure of Riemannian manifold in the space of unitaries representing all the possible quantum circuits and, therefore, makes it easier to find the optimal path. For this reason more tools, such as formula (2.60), are present in literature to handle the problem of complexity with an F_2 cost function. However, there is no clear agreement whether to choose F_2 rather than other cost functions, such as F_1 or the other ones listed in expression (2.16) [6]. Therefore, in the future it would be interesting to extend our analysis to other kind of cost functions.

We focused on the family of quantum circuits in expression (4.2) which connect the ground state of the free bosonic harmonic chain to the ground state of the harmonic chain with defect. Such choice is very peculiar and differs from what has been done in most of the literature regarding complexity starting from [6]. The state which is commonly taken as the reference, is the maximally unentangled one, defined in section 2.2. In our case, making this choice for the reference state makes the complexity in presence of defect equal to the complexity for the simple free bosonic theory obtained in [6], as it has been clarified in section 3.5. However, there is no clear agreement on which should be the correct reference state to make comparisons with holography [6, 103, 104]. Hence, we were naturally led to study the class of paths in (4.2), which does not depend on the peculiar choice of the reference state. This makes us able to derive an upper bound - see formula (6.30) - on the difference between the complexity associated to the ground state with and without defect, avoiding to make any assumption on the specific nature of the reference state.

We managed to extract the divergence structure of $\mathcal{C}_2$ complexity in the continuum limit defined in section 4.1. We performed this study in two different basis for the Hamiltonian of the harmonic chain with defect and saw a practical demonstration that if the change of basis is performed only in the target state, it affects dramatically the structure of $\mathcal{C}_2$ complexity. The divergence pattern is volumic if we adopt Extended Coordinates, whereas it is logarithmic if we choose Localized Coordinates. This is due to the fact that in the Extended Basis the effect of the defect is spread through the chain, whereas in Localized Basis it is limited to the contact point between the two sides of the defect. For this reason we expected the divergence in Localized Coordinates to be weaker than that in Extended Coordinates.

We consider the presence of a logarithmic divergence pattern in Localized

Coordinates to be the main result of our thesis. From now on, we will refer only to the $\mathcal{C}_2$ divergence structure in Localized Coordinates, unless specified. Such divergence structure is certainly present in the massive case and seems to remain also in the limit of massless field theory. Even if we cannot take rigorously the massless continuum limit, because of the presence of a zero mode in the spectrum, our analysis strongly indicates that the logarithmic structure in the divergence pattern of complexity is present also in the massless case. It would be interesting to repeat the same analysis with different boundary conditions for our harmonic chain, for example Dirichlet ones, allowing us to set sharply to zero the mass parameter of our defect harmonic chain. This has already been done in the case without the defect [12], and could be extended to the harmonic chain with defect studied in this thesis with Dirichlet boundary conditions. Moreover, another interesting extension would consist in studying the complexity associated to a subregion of the harmonic chain with defect, using the tools developed in [23–27]. In particular, it would be possible to consider various subregions: one containing the defect, one without the defect and one with an endpoint on the defect locus.

The presence of a logarithmic divergence in the continuum limit of $\mathcal{C}_2$ complexity recalls the presence of another logarithmic divergence in the entanglement entropy associated to a subregion of a conformal field theory in $1+1$ dimension [78–81]. It was already known that such logarithmic divergence holds also in the continuum limit of the massless harmonic chain with defect in section 3 and an exact result had been derived for the coefficient $c_{eff}(\theta)$ in front of the logarithmic divergence [62, 83], showing its dependence on the strength of the defect θ. We managed to reconstruct numerically the logarithmic divergence of the half chain with defect entangelment entropy in the continuum limit and studied the coefficient $c(\theta)$ in (5.31). We found that as the strength of the defect θ increases, the theoretical result $c_{eff}(\theta)$ does not match with the one extracted from our numerical results $c(\theta)$ in the massless limit. It would be nice to better understand the origin of this discrepancy, which was expected as it had been already mentioned in [62].

In order to investigate a possible relation between the logarithmic divergence of the entanglement entropy and that of $\mathcal{C}_2$ complexity, we reconstructed numerically the coefficient of the logarithmic divergence $a(\theta)$ as function of θ. The outcome is that there seems to be almost no relation between $c(\theta)$ and $a(\theta)$. Nevertheless, we consider our effort to find $a(\theta)$ worth because we provided a numerical results which can be used as a reference if one day a method is found to derive $a(\theta)$ analytically in the framework of defect quantum field theory. It would be nice to see if the techniques used in [62] can be extended to the continuum limit of $\mathcal{C}_2$ complexity for the harmonic chain with defect.

In the last part of this thesis, we observed that our results for $\mathcal{C}_2$ complexity in the continuum limit of the harmonic chain with defect could be compared to those obtained in a holographic set up in presence of defect [75]. It should be

remembered that such comparison is not the best possible because according to the AdS/CFT correspondence, we should compute complexity in a strongly interacting defect CFT, whereas we are working in a free theory. Nevertheless, it represents the best that we can do with the techniques that have been developed up to date to calculate complexity. The key result in [75] for holographic complexity in presence of defect is that a subleading logarithmic divergence arises only in the $\mathcal{CV}$ conjecture, whereas in the $\mathcal{CA}$ case holographic complexity is not affected by the presence of the defect. If we look at $\mathcal{C}_2$ for the ground state of the harmonic chain with defect with respect to the maximally unentangled reference state, we are soon led to conclude that $\mathcal{CA}$ conjecture is supported by our calculations.

However, we managed to learn a more general lesson from our calculations in a way which is independent from the choice of the reference state. Let us consider the difference between holographic complexity with and without defect. As it is clear from inequality (6.31), the quantum field theory dual of this quantity is upper bounded by the complexity of the quantum circuit going from the ground state of the boundary quantum field theory without defect to that in presence of defect. We notice that such quantity might display a similar UV divergence pattern as the complexity that we studied numerically in this thesis. Therefore, we are led to conclude that, if we restrict to $\mathcal{C}_2$ complexity and assume nothing about the reference state, the subleading divergence associated to the defect can be at most logarithmic. This result is compatible with the holographic complexity in presence of defect obtained in both conjectures. In the future, it would be interesting to see if this result holds also using other cost functions or it is specific of $\mathcal{C}_2$. It has been pointed out by the authors of [75] that the different results in $\mathcal{CV}$ and $\mathcal{CA}$ for the holographic complexity in presence of defect might correspond to a different choice of the cost function. This claim still needs to be tested. Another interesting question to be explored in the future regards the divergence pattern of holographic complexity in presence of defect in a $AdS_3/BCFT_2$ set up [105, 106] and the match with the continuum limit of $\mathcal{C}_2$ for the harmonic chain with defect in presence of boundary.

In conclusion, the study of complexity in presence of defect is a very important and promising tool to test the validity of $\mathcal{CV}$ and $\mathcal{CA}$ conjectures and to understand differences and analogy between the two of them. Our investigations showed that the continuum limit of $\mathcal{C}_2$ complexity for the ground state of the harmonic chain with defect is compatible with the corresponding holographic complexity in both conjectures $\mathcal{CV}$ and $\mathcal{CA}$, up to a suitable choice of the reference state. In this way we think that this thesis provided further evidence of how the study of complexity in presence of defect might help to take further steps in the search for the holographic dual to the complexity of the boundary quantum field theory .

Besides that, the road to a rigorous quantum field theory definition for

complexity is still long and far from its end. Our results provide a confirm of the power of the lattice field theory approach to complexity, since they might serve as guide in the search for an analytic derivation of complexity in a defect quantum field theory. Moreover, we believe that all the techniques developed in this thesis can be easily adapted to other problems and used to answer some of the new questions about complexity which will inevitably arise in the close future.

A Correlators in the Harmonic Chain with Defect

Explicit Form of Correlators for the Hamiltonian on a Segment We rewrite correlators in expressions (3.46) and (3.47) such a way that their dependence on the defect strength is made explicit. We will focus on the case where the chain is defined on a segment, whose Hamiltonian is given by equations (3.1) and (3.7). We will report between square brackets the multiplicative modification that occurs to the result when we move from Localized Coordinates to Extended Coordinates. In the case where both points are in the first half chain, $i \in \{1,\dots,L\}$ and $j \in \{1,\dots,L\}$, we have that:

$$\begin{aligned}\langle x_i x_j\rangle &= \left[\frac{1}{m_1}\right]\sum_{n=1}^{2L}\frac{1}{2\Omega_n}\alpha_n^2\Phi_n^{hom}(i)\Phi_n^{hom}(j) = \\ &= \left[\frac{1}{e^{\theta}}\right]\sum_{n=1}^{2L}\left(1+(-)^{n+1}\tanh\theta\right)\frac{\Phi_n^{hom}(i)\Phi_n^{hom}(j)}{2\Omega_n},\end{aligned} \tag{A.1}$$

whereas if they belong to two different half chains, i.e. $i \in 1,\dots,L$ and $j \in L+1,\dots,2L$, we obtain that:

$$\begin{aligned}\langle x_i x_j\rangle &= \sum_{n=1}^{2L}\frac{1}{2\Omega_n}\alpha_n\beta_n\Phi_n^{hom}(i)\Phi_n^{hom}(j) = \\ &= \frac{1}{\cosh\theta}\sum_{n=1}^{2L}\frac{\Phi_n^{hom}(i)\Phi_n^{hom}(j)}{2\Omega_n},\end{aligned} \tag{A.2}$$

where we have just used (3.19). Finally, we consider the case where the two points are both in the last half chain, namely $i \in \{L+1,\dots,2L\}$ and $j \in \{L+1,\dots,2L\}$:

$$\begin{aligned}\langle x_i x_j\rangle &= \left[\frac{1}{m_2}\right]\sum_{n=1}^{2L}\frac{1}{2\Omega_n}\beta_n^2\Phi_n^{hom}(i)\Phi_n^{hom}(j) = \\ &= \left[\frac{1}{e^{-\theta}}\right]\sum_{n=1}^{2L}\left(1+(-)^{n}\tanh\theta\right)\frac{\Phi_n^{hom}(i)\Phi_n^{hom}(j)}{2\Omega_n}.\end{aligned} \tag{A.3}$$

Explicit Form of Correlators for Hamiltonian on a Circle We now consider the Hamiltonian defined on a circle with two defect points, which is represented by Hamiltonians in formulas (C.1) and (C.2). In the case where both points are in the same half chain, $i \in \{0,\dots,L-1\}\cup\{3L,\dots,4L-1\}$ and $j \in \{1,\dots,L\}\cup\{3L,\dots,4L-1\}$, we have that:

$$\begin{aligned}\langle x_i x_j\rangle &= \left[\frac{1}{m_1}\right]\sum_{n=0}^{4L-1}\frac{\alpha_n^2}{2\Omega_n}\Phi_n^{hom}(i)\Phi_n^{hom}(j) = \\ &= \left[\frac{1}{e^{\theta}}\right]\sum_{n=0}^{4L-1}\left(1+(-)^{n}\tanh\theta\right)\frac{\Phi_n^{hom}(i)\Phi_n^{hom}(j)}{2\Omega_n},\end{aligned} \tag{A.4}$$

whereas if they belong to two different half chains, i.e. $i \in \{0,\dots,L-1\} \cup \{3L,\dots,4L-1\}$ and $j \in \{L,\dots,3L-1\}$, we obtain that:

$$\begin{aligned}\langle x_i x_j \rangle &= \sum_{n=0}^{4L-1} \frac{\alpha_n \beta_n}{2\Omega_n} \Phi_n^{hom}(i)\Phi_n^{hom}(j) = \\ &= \frac{1}{\cosh\theta} \sum_{n=0}^{4L_1} \frac{\Phi_n^{hom}(i)\Phi_n^{hom}(j)}{2\Omega_n},\end{aligned} \tag{A.5}$$

where we have just used (3.19). Finally, we consider the case where the two points are both in the other half chain, namely $i \in \{L,\dots,3L-1\}$ and $j \in \{L,\dots,3L-1\}$:

$$\begin{aligned}\langle x_i x_j \rangle &= \left[\frac{1}{m_2}\right] \sum_{n=0}^{4L-1} \frac{1}{2\Omega_n} \beta_n^2 \Phi_n^{hom}(i)\Phi_n^{hom}(j) = \\ &= \left[\frac{1}{e^{-\theta}}\right] \sum_{n=0}^{4L-1} \left(1 + (-)^{n+1} \tanh\theta\right) \frac{\Phi_n^{hom}(i)\Phi_n^{hom}(j)}{2\Omega_n}.\end{aligned} \tag{A.6}$$

Explicit Results for Correlators in Linear Approximation We expose some explicit calculations for the first order Taylor expansion as defined in (3.52) for correlators in expressions in formulas (A.1), (A.2) and (A.3). We focus on the case of the chain defined on a segment described in section 3.1. In the case where both points are in the first half chain, $i \in \{1,\dots,L\}$ and $j \in \{1,\dots,L\}$, we have that:

$$\langle x_i x_j \rangle \simeq \sum_{n=1}^{2L} \frac{\Phi_n^{hom}(i)\Phi_n^{hom}(j)}{2\Omega_n} + \theta \sum_{n=1}^{2L} (-)^{n+1} \frac{\Phi_n^{hom}(i)\Phi_n^{hom}(j)}{2\Omega_n} + O(\theta^2), \tag{A.7}$$

whereas if they belong to two different half chains, i.e. $i \in \{1,\dots,L\}$ and $j \in \{L+1,\dots,2L\}$, we obtain that:

$$\langle x_i x_j \rangle \simeq \sum_{n=1}^{2L} \frac{\Phi_n^{hom}(i)\Phi_n^{hom}(j)}{2\Omega_n} + O(\theta^2). \tag{A.8}$$

Finally, we consider the case where the two points are both in the last half chain, namely $i \in \{L+1,\dots,2L\}$ and $j \in \{L+1,\dots,2L\}$:

$$\langle x_i x_j \rangle \simeq \sum_{n=1}^{2L} \frac{\Phi_n^{hom}(i)\Phi_n^{hom}(j)}{2\Omega_n} + \theta \sum_{n=1}^{2L} (-)^{n} \frac{\Phi_n^{hom}(i)\Phi_n^{hom}(j)}{2\Omega_n} + O(\theta^2), \tag{A.9}$$

Summing up, we obtain:

$$G_{lin} = \mathcal{X}_{lin} \oplus \mathcal{P}_{lin}, \tag{A.10}$$

where we have that:

$$\mathcal{X}_{lin} = \left[\begin{array}{c|c} \left(\sum_{n=1}^{2L}(-)^{n+1}\ \frac{\Phi_n^{hom}(i)\Phi_n^{hom}(j)}{2\Omega_n}\right)_{ij} & 0 \\ \hline 0 & \left(\sum_{n=1}^{2L}(-)^{n}\frac{\Phi_n^{hom}(i)\Phi_n^{hom}(j)}{2\Omega_n}\right)_{ij} \end{array}\right], \tag{A.11}$$

$$\mathcal{P}_{lin} = \left[\begin{array}{c|c} \left(\sum_{n=1}^{2L}(-)^{n+1}\ \frac{\Omega_n}{2}\Phi_n^{hom}(i)\Phi_n^{hom}(j)\right)_{ij} & \prime \\ \hline \prime & \left(\sum_{n=1}^{2L}(-)^{n}\frac{\Omega_n}{2}\Phi_n^{hom}(i)\Phi_n^{hom}(j)\right)_{ij} \end{array}\right]. \tag{A.12}$$

B Convergence of Complexity in Continuum Limit

We want to show that if we take the quantum field theory limit as defined in section 4.1, the convergence of $\mathcal{C}_2$ in the case of the pure state is practically reached when the number of chain sites is $2L > 1400$. We first show it qualitatively in figure 18 where we focus on the case $2\Omega_0 L = 10^{-4}$ and we perform the fit in several subsequent ranges of $2L$ with steps of 20 sites:

$$\begin{aligned} 2L \in \{&[200, 1800], [400, 1800], [600, 1800], [800, 1800], \\ &[1000, 1800], [1200, 1800], [1400, 1800], [1600, 1800]\}. \end{aligned} \tag{B.1}$$

As we can see the curve for $a(\theta)$ coefficient, defined in equation (4.5), collapses to its asymptotic behavior which can be considered almost reached when $2L \in [1600, 1800]$. From now on we will call the fitted value for $a(\theta)$ in this range as $\tilde{a}(\theta)$.
Secondly, we compute the following ratio:

$$\mathcal{R} = \frac{a(\theta) - \tilde{a}(\theta)}{\tilde{a}(\theta)}, \tag{B.2}$$

where $a(\theta)$ is computed for $2L$ in one of the ranges specified in B.1 and $\tilde{a}(\theta)$ is computed for $2L$ in the range $[1600, 1800]$. In figure 19, we focus on the case $2\Omega_0 L = 10^{-4}$ and plot $\mathcal{R}(\theta)$ as a function of θ for the various ranges of $2L$. We can clearly see that $\mathcal{R}(\theta)$ is always below than 1% for $2L > 1400$. Even if we do not show plots, analogous results yield for the other values of $2\Omega_0 L$.

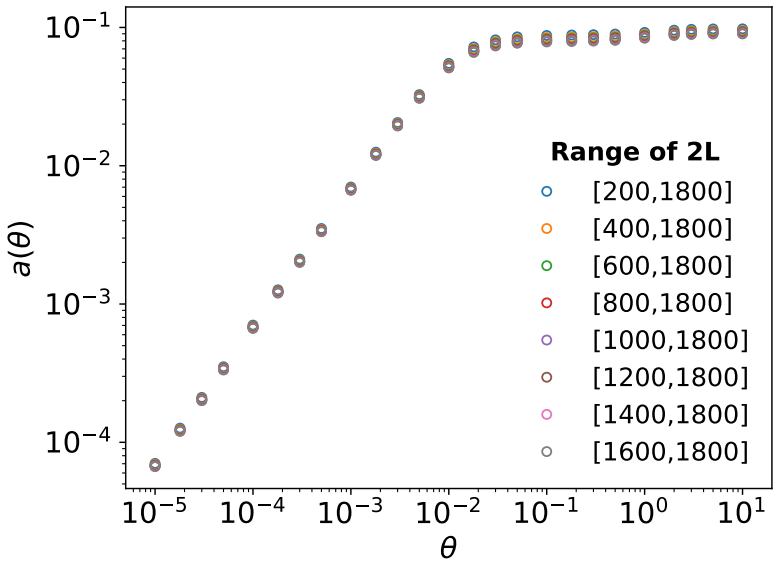

(a) $a(\theta)$- *Logarithmic Plot*

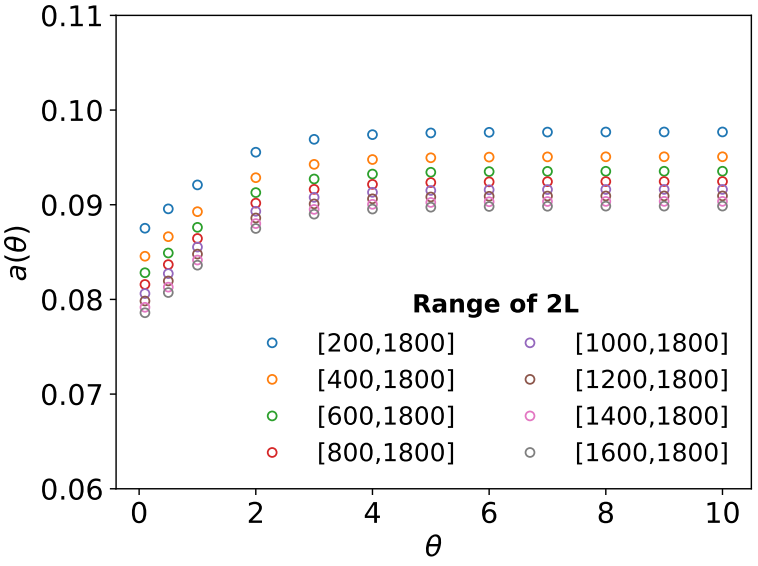

(b) $a(\theta)$- *Saturation Plot*

Figure 18: Coefficient $a(\theta)$ in QFT limit at fixed $2\Omega_0 L = 10^{-4}$.

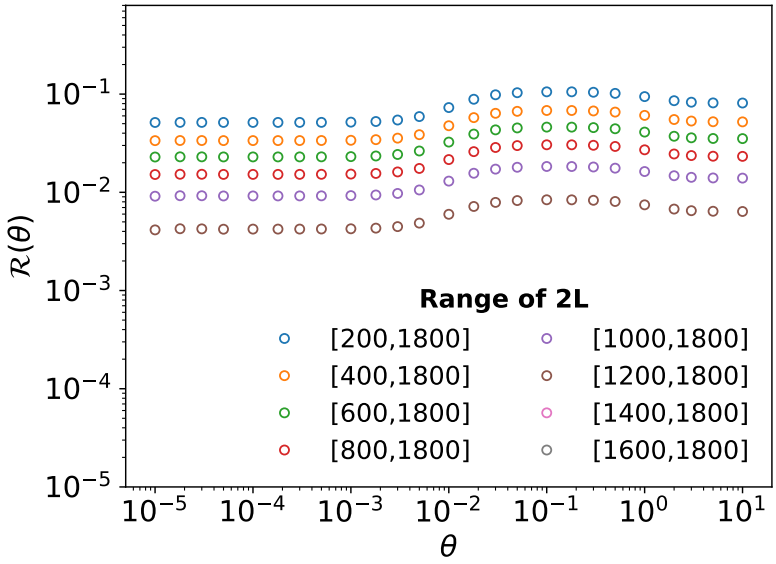

Figure 19: Coefficient $\mathcal{R}(\theta)$ in formula (B.2) at fixed $2\Omega_0 L = 10^{-4}$.

C Harmonic Chain with two Defects on a Circle

Harmonic Chain with Defect on a Circle

We consider now a harmonic chain defined on circle of length $4L$ where the defect is located in two different points which are equally distant from each other on both sides . Such system is represented in figure 20 and represents a straightforward extension of that analyzed by Eisler and Peschel in [62].

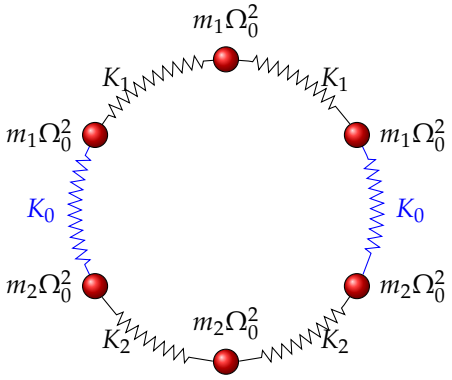

Figure 20: Harmonic Chain with Defect.Periodic Boundary Conditions.

For completeness we report the system Hamiltonian in the Extended Basis:

$$
\begin{aligned}
H = & \sum_{n=0}^{L-1}\left(\frac{p_n^2}{2m_1}+\frac{1}{2}m_1\Omega_0^2x_n^2\right)+\sum_{n=0}^{L-2}\left(\frac{m_1}{2}(x_n-x_{n+1})^2\right)+ \\
& +\frac{1}{2}K_0\,(x_{L-1}-x_L)^2+ \\
& +\sum_{n=L}^{3L-1}\left(\frac{p_n^2}{2m_2}+\frac{1}{2}m_2\Omega_0^2x_n^2\right)+\sum_{n=L}^{3L-1}\left(\frac{m_1}{2}(x_n-x_{n+1})^2\right) \\
& +\frac{1}{2}K_0\,(x_{3L-1}-x_{3L})^2+ \\
& +\sum_{n=3L}^{4L-1}\left(\frac{p_n^2}{2m_2}+\frac{1}{2}m_2\Omega_0^2x_n^2\right)+\sum_{n=3L}^{4L-1}\left(\frac{m_1}{2}(x_n-x_{n+1})^2\right),
\end{aligned}
\tag{C.1}
$$

as well as in the Localized Basis:

$$
\begin{aligned}
H = &\sum_{n=0}^{4L-1}\left(\frac{p_n^2}{2}+\frac{1}{2}\Omega_0^2 x_n^2\right)+\sum_{n=0}^{4L-1}\left(\frac{1}{2}(x_n-x_{n+1})^2\right)+\\
&+\frac{1}{2}\frac{K_0}{m_1}x_{L-1}^2+\frac{1}{2}\frac{K_0}{m_2}x_L^2-K_0x_{L-1}x_L\\
&+\frac{1}{2}\frac{K_0}{m_1}x_{3L-1}^2+\frac{1}{2}\frac{K_0}{m_2}x_{3L}^2-K_0x_{3L-1}x_{3L}.
\end{aligned}
\tag{C.2}
$$

The quantities K_0, Ω_0, m_1 and m_2 are those defined in the previous section.

Spectrum of the Harmonic Chain on a Circle with Defect

We will briefly show that the with a procedure analogous to that in section 3.2, we can find the spectrum for the Hamiltonian in formulas (C.1) and (C.2).

Homogeneous Problem We report the spectrum of the homogeneous harmonic chain with 4L sites following the conventions introduced in section 7 of [107]. The eigenvalues are:

$$
\Omega_m^{2\ hom}=\Omega_0^2+4\left(\sin\frac{m\pi}{4L}\right)^2 \qquad m\in\{0,\dots,4L-1\}, \tag{C.3}
$$

whereas the eigenfunctions read:

$$
\Phi_m^{hom}(n)=\sqrt{\frac{1}{4L}}e^{-\frac{2\pi mn}{4L}i} \qquad m,n\in\{0,\dots,4L-1\}. \tag{C.4}
$$

Inhomogeneous Problem We make the ansatz that the spectrum stays the same:

$$
\Omega_m=\Omega_m^{hom}, \tag{C.5}
$$

whereas the eigenfunctions are modified with a defect dependent factor:

$$
\Phi_m(n)=\begin{cases}\alpha_m\Phi_m^{hom}(n) & n\in\{0,\dots,L-1\}\\ \beta_m\Phi_m^{hom}(n) & n\in\{L,\dots,3L-1\}\\ \alpha_m\Phi_m^{hom}(n) & n\in\{3L,\dots,4L-1\}\end{cases} \qquad \alpha_m\in\mathbb{R},\ \beta_m\in\mathbb{R}. \tag{C.6}
$$

We find α_m and β_m imposing the orthonormality condition and the eigenvalue equation at the defect interface as it was done in section (3.2), taking care of the fact that in this case the defect interfaces are two, located between L-1 and L sites and between 3L-1 and 3L sites. We finally find that:

$$
\alpha_m^2=1+(-)^m\tanh\theta \qquad m\in\{0,\dots,L-1\}\cup\{3L,\dots,4L-1\}, \tag{C.7}
$$

$$
\beta_m^2=1+(-)^{m+1}\tanh\theta \qquad m\in\{L\dots3L-1\}. \tag{C.8}
$$

$$
\tag{C.9}
$$

Correlators for the Harmonic Chain on a Circle with Defect

We wish to transform the Hamiltonian in equations (C.1) and (C.2) into the Hamiltonian of a chain of decoupled oscillators, through a canonical transformation. Then, we wish to define a second quantization Hamiltonian as in equation (C.14) and to find the change of basis connecting our dynamical variables to second quantization operators.

Structure of the Orthogonal Change of Basis We wish to define the orthogonal matrix $P_{ij}(\theta)$, which induces the following change of basis:

$$\begin{bmatrix} \tilde{\vec{x}} \\ \tilde{\vec{p}} \end{bmatrix} = \begin{bmatrix} P(\theta)^T & 0 \\ 0 & P(\theta)^T \end{bmatrix} \begin{bmatrix} \vec{x} \\ \vec{p} \end{bmatrix}. \tag{C.10}$$

such that:

- it is canonical;
- it reshapes the Hamiltonian of our problem in this way:

$$H = \frac{1}{2} \sum_{i=1}^{2L} \left(\tilde{p}_i^2 + \Omega_i^2 \tilde{x}_i \right). \tag{C.11}$$

If we consider the Hamiltonian in its Localized Basis (C.2), the matrix $P(\theta)$, containing on the columns the eigenvectors, has the following form:

$$P_{ij}(\theta) = \mathcal{D}_{ij}(\theta) \Phi_j^{hom}(i). \tag{C.12}$$

The coefficient $\mathcal{D}_{ij}(\theta)$ encloses the dependence from the defect and on the cricle reads:

$$\mathcal{D}_{ij}(\theta)|_{circle} = \begin{cases} \sqrt{1 + (-)^j \tanh\theta} & i \in \{0, \dots, L-1\} \cup \{3L, \dots, 4L-1\} \\ \sqrt{1 + (-)^{j+1} \tanh\theta} & i \in \{L, \dots, 3L-1\} \end{cases}. \tag{C.13}$$

Second Quantization Hamiltonian At this point is possible to write the Hamiltonian above in terms of the second quantization operators:

$$H = \sum_{i=1}^{4L} \Omega_i \left(\hat{a}_i^\dagger \hat{a}_i + \frac{1}{2} \right), \tag{C.14}$$

where:

$$\hat{a}_i = \sqrt{\frac{\Omega_i}{2}} \left(\tilde{x}_i + i \frac{\tilde{p}_i}{\Omega_i} \right), \qquad \hat{a}_i^\dagger = \sqrt{\frac{\Omega_i}{2}} \left(\tilde{x}_i - i \frac{\tilde{p}_i}{\Omega_i} \right). \tag{C.15}$$

We can build up a closed expression for the change of basis connecting the operators x_i and p_i figuring in the original Hamiltonian, either in the Extended Basis or in the Localized Basis, to the second quantization operators $\hat{a}_i$ and $\hat{a}_i^\dagger$, using a completely analogous procedure to that used in section 3.3:

$$\begin{cases} x_i = \sum_{j=1}^{4L} \left[\frac{1}{\sqrt{m_i}}\right] \frac{1}{\sqrt{2\Omega_j}} \mathcal{D}_{ij}(\theta) \Phi_j^{hom}(i) \left(\hat{a}_j + \hat{a}_j^\dagger\right) \\ p_i = \sum_{j=1}^{4L} \left[\sqrt{m_i}\right] \sqrt{\frac{\Omega_j}{2}} \frac{1}{i} \mathcal{D}_{ij}(\theta) \Phi_j^{hom}(i) \left(\hat{a}_j - \hat{a}_j^\dagger\right) \end{cases}, \tag{C.16}$$

where the terms in the squared brackets are multiplicative factors which appear only when we use the Extended Basis. Even in this case, the dependence on the defect strength θ is all contained in the masses m_i, which appear only in the case we use the Extended Basis, and in the matrix $\mathcal{D}_{ij}(\theta)$.

General Form of Correlators We can build the 2-points correlator for positions and momenta, $\langle x_i x_j \rangle$ and $\langle p_i p_j \rangle$ using a procedure analogous to that in section 3.4. We obtain the following results analogous to those obtained for the Hamiltonian on a segment in equations (3.46) and (3.47):

$$\langle x_i x_j \rangle = \left[\frac{1}{\sqrt{m_i m_j}}\right] \sum_{n=1}^{4L} \frac{1}{2\Omega_n} \mathcal{D}_{in}(\theta) \mathcal{D}_{jn}(\theta) \Phi_n^{hom}(i) \Phi_n^{hom}(j), \tag{C.17}$$

$$\langle p_i p_j \rangle = \left[\sqrt{m_i m_j}\right] \sum_{n=1}^{4L} \frac{\Omega_n}{2} \mathcal{D}_{in}(\theta) \mathcal{D}_{jn}(\theta) \Phi_n^{hom}(i) \Phi_n^{hom}(j), \tag{C.18}$$

where the terms in the square brackets are the multiplicative factors which appear if we consider the Extended Basis.

Covariance Matrix Then, our covariance matrix G is the $8L \times 8L$ block diagonal matrix:

$$G = \left[\begin{array}{c|c} \mathcal{X} & \\ \hline & \mathcal{P} \end{array}\right], \tag{C.19}$$

where:

$$\mathcal{X} = \begin{bmatrix} x_{1,1} & \dots & x_{1,4L} \\ \vdots & \ddots & \vdots \\ x_{4L,1} & \dots & x_{4L,4L} \end{bmatrix}, \qquad \mathcal{P} = \begin{bmatrix} p_{1,1} & \dots & p_{1,4L} \\ \vdots & \ddots & \vdots \\ p_{4L,1} & \dots & p_{4L,4L} \end{bmatrix}. \tag{C.20}$$

We can rewrite the covariance matrix in this form:

$$G_T = \frac{1}{2} \left(P(\theta) \Omega^{-1} P(\theta) \oplus P(\theta) \Omega P(\theta) \right), \tag{C.21}$$

where $P(\theta)$ is defined by condition (3.34) and Ω is the diagonal matrix containing the spectrum of the Hamiltonian:

$$\Omega = diag(\Omega_1, \dots, \Omega_{4L}). \tag{C.22}$$

Acknowledgements

As I approach to my last days in Padova as a Master student, I look back to all the moments of my past two years and simply realize that it is impossible to enclose in those few lines all the people that left their footprint along my path. Those who I am going to mention below are only some of the people who deserve to appear in this paragraph.

First of all, I would like to thank prof. Erik Tonni for being an enlightening guide in my first steps towards the world of research. I want to thank him for his patience, for all time that he dedicated me in our Zoom meetings, and, mostly, for transmitting me all the passion and the enthusiasm towards theoretical physics. I am really honored that he will continue to be my supervisor in my PhD. I would like also to thank my internal supervisor prof.Alessandro Sfondrini, for his kindness and the precious advice that he gave me in my path towards the Master degree. A big part of my gratitude goes to Giuseppe Di Giulio, who assisted prof.Tonni in the supervision of this thesis, and without whom this project would have never been possible. I really enjoyed our online conversations and I hope I will have the chance to work with him in the future.

I wish to thank the Physics Department of the University of Padova and Galilean School of Higher Education, which are the two institutions where I have grown as a physics student and as a person. In particular, I would like to thank my laboratory mates - who had to suffer the presence of a theoretician in their group, - and all the friends from the group *Joůœūördœn* - who were always ready to share a spritz (even more than one). I am grateful also to my fellow Galilean students, especially to those belonging to the 13^{th} cohort and to those living at the $4B$ floor of our dormitory, who were almost tolerant with my cooking habits.

Finally, I want to thank my family for being supportive and for helping me throughout these years. I am really grateful to them for always giving me a place where I can return.

Francesco

References

[1] J. Watrous. Quantum Computational Complexity. *Encyclopedia of Complexity and Systems Science*, pages 7174–7201, 2009.

[2] Scott Aaronson. The Complexity of Quantum States and Transformations: From Quantum Money to Black Holes. 7 2016.

[3] Michael A. Nielsen. A Geometric Approach to Quantum Circuit Lower Bounds. *Quantum Info. Comput.*, 6(3):213–262, 2006.

[4] Michael A. Nielsen, Mark R. Dowling, M. Gu, and A. Doherty. Quantum computation as geometry. *Science*, 311(5764):1133–1135, 2006.

[5] Mark R. Dowling and Michael A. Nielsen. The Geometry of Quantum Computation. *Quantum Info. Comput.*, 8(10):861–899, 2008.

[6] Ro Jefferson and Robert C. Myers. Circuit complexity in quantum field theory. *JHEP*, 10:107, 2017.

[7] Shira Chapman, Michal P. Heller, Hugo Marrochio, and Fernando Pastawski. Toward a Definition of Complexity for Quantum Field Theory States. *Phys. Rev. Lett.*, 120(12):121602, 2018.

[8] Shira Chapman, Jens Eisert, Lucas Hackl, Michal P. Heller, Ro Jefferson, Hugo Marrochio, and Robert C. Myers. Complexity and entanglement for thermofield double states. *SciPost Phys.*, 6(3):034, 2019.

[9] Minyong Guo, Juan Hernandez, Robert C. Myers, and Shan-Ming Ruan. Circuit Complexity for Coherent States. *JHEP*, 10:011, 2018.

[10] Lucas Hackl and Robert C. Myers. Circuit complexity for free fermions. *JHEP*, 07:139, 2018.

[11] Rifath Khan, Chethan Krishnan, and Sanchita Sharma. Circuit Complexity in Fermionic Field Theory. *Phys. Rev. D*, 98(12):126001, 2018.

[12] Paolo Braccia, Aldo L. Cotrone, and Erik Tonni. Complexity in the presence of a boundary. *JHEP*, 02:051, 2020.

[13] Shira Chapman and Hong Zhe Chen. Charged Complexity and the Thermofield Double State. *JHEP*, 02:187, 2021.

[14] Mehregan Doroudiani, Ali Naseh, and Reza Pirmoradian. Complexity for Charged Thermofield Double States. *JHEP*, 01:120, 2020.

[15] Minyong Guo, Zhong-Ying Fan, Jie Jiang, Xiangjing Liu, and Bin Chen. Circuit complexity for generalized coherent states in thermal field dynamics. *Phys. Rev. D*, 101(12):126007, 2020.

[16] Nitesh Jaiswal, Mamta Gautam, and Tapobrata Sarkar. Complexity and information geometry in spin chains. 5 2020.

[17] Alessandro Ferraro, Stefano Olivares, and Matteo G. A. Paris. Gaussian states in continuous variable quantum information, 2005.

[18] A. Holevo. *Probabilistic and Statistical Aspects of Quantum Theory*. Edizioni della Normale, 2011.

[19] Christian Weedbrook, Stefano Pirandola, Raúl García-Patrón, Nicolas J. Cerf, Timothy C. Ralph, Jeffrey H. Shapiro, and Seth Lloyd. Gaussian quantum information. *Rev. Mod. Phys.*, 84(2):621–669, 2012.

[20] Gerardo Adesso, Sammy Ragy, and Antony R. Lee. Continuous Variable Quantum Information: Gaussian States and Beyond. *Open Systems and Information Dynamics*, 21(01n02):1440001, 2014.

[21] A. Serafini. *Quantum Continuous Variables: A Primer of Theoretical Methods*. CRC Press, 2017.

[22] Dorit Aharonov, Alexei Kitaev, and Noam Nisan. Quantum circuits with mixed states, 1998.

[23] Cesar A. Agón, Matthew Headrick, and Brian Swingle. Subsystem Complexity and Holography. *JHEP*, 02:145, 2019.

[24] Elena Caceres, Shira Chapman, Josiah D. Couch, Juan P. Hernandez, Robert C. Myers, and Shan-Ming Ruan. Complexity of Mixed States in QFT and Holography. *JHEP*, 03:012, 2020.

[25] Giuseppe Di Giulio and Erik Tonni. Complexity of mixed Gaussian states from Fisher information geometry. *JHEP*, 12:101, 2020.

[26] Shan-Ming Ruan. Purification Complexity without Purifications. *JHEP*, 01:092, 2021.

[27] Hugo A. Camargo, Lucas Hackl, Michal P. Heller, Alexander Jahn, Tadashi Takayanagi, and Bennet Windt. Entanglement and complexity of purification in (1+1)-dimensional free conformal field theories. *Phys. Rev. Res.*, 3(1):013248, 2021.

[28] Arpan Bhattacharyya, Arvind Shekar, and Aninda Sinha. Circuit complexity in interacting QFTs and RG flows. *JHEP*, 10:140, 2018.

[29] Pawel Caputa, Nilay Kundu, Masamichi Miyaji, Tadashi Takayanagi, and Kento Watanabe. Anti-de Sitter Space from Optimization of Path Integrals in Conformal Field Theories. *Phys. Rev. Lett.*, 119(7):071602, 2017.

[30] Bartlomiej Czech. Einstein Equations from Varying Complexity. *Phys. Rev. Lett.*, 120(3):031601, 2018.

[31] Pawel Caputa, Nilay Kundu, Masamichi Miyaji, Tadashi Takayanagi, and Kento Watanabe. Liouville Action as Path-Integral Complexity: From Continuous Tensor Networks to AdS/CFT. *JHEP*, 11:097, 2017.

[32] Pawel Caputa and Javier M. Magan. Quantum Computation as Gravity. *Phys. Rev. Lett.*, 122(23):231302, 2019.

[33] Arpan Bhattacharyya, Pawel Caputa, Sumit R. Das, Nilay Kundu, Masamichi Miyaji, and Tadashi Takayanagi. Path-Integral Complexity for Perturbed CFTs. *JHEP*, 07:086, 2018.

[34] Hugo A. Camargo, Michal P. Heller, Ro Jefferson, and Johannes Knaute. Path integral optimization as circuit complexity. *Phys. Rev. Lett.*, 123(1):011601, 2019.

[35] Dongsheng Ge and Giuseppe Policastro. Circuit Complexity and 2D Bosonisation. *JHEP*, 10:276, 2019.

[36] Mario Flory and Michal P. Heller. Conformal field theory complexity from Euler-Arnold equations. *JHEP*, 12:091, 2020.

[37] Johanna Erdmenger, Marius Gerbershagen, and Anna-Lena Weigel. Complexity measures from geometric actions on Virasoro and Kac-Moody orbits. *JHEP*, 11:003, 2020.

[38] Mario Flory and Michal P. Heller. Geometry of Complexity in Conformal Field Theory. *Phys. Rev. Res.*, 2(4):043438, 2020.

[39] Nicolas Chagnet, Shira Chapman, Jan de Boer, and Claire Zukowski. Complexity for Conformal Field Theories in General Dimensions. 3 2021.

[40] Leonard Susskind. The world as a hologram. *Journal of Mathematical Physics*, 36(11):6377–6396, may 1995.

[41] Gerard 't Hooft. Dimensional reduction in quantum gravity. 1993.

[42] Juan Martin Maldacena. The Large N limit of superconformal field theories and supergravity. *Int. J. Theor. Phys.*, 38:1113–1133, 1999.

[43] Edward Witten. Anti-de Sitter space and holography. *Adv. Theor. Math. Phys.*, 2:253–291, 1998.

[44] S.S. Gubser, Igor R. Klebanov, and Alexander M. Polyakov. Gauge theory correlators from noncritical string theory. *Phys. Lett. B*, 428:105–114, 1998.

[45] Ofer Aharony, Steven S. Gubser, Juan Martin Maldacena, Hirosi Ooguri, and Yaron Oz. Large N field theories, string theory and gravity. *Phys. Rept.*, 323:183–386, 2000.

[46] Shinsei Ryu and Tadashi Takayanagi. Holographic derivation of entanglement entropy from AdS/CFT. *Phys. Rev. Lett.*, 96:181602, 2006.

[47] Shinsei Ryu and Tadashi Takayanagi. Aspects of Holographic Entanglement Entropy. *JHEP*, 08:045, 2006.

[48] Veronika E. Hubeny, Mukund Rangamani, and Tadashi Takayanagi. A Covariant holographic entanglement entropy proposal. *JHEP*, 07:062, 2007.

[49] Tatsuma Nishioka, Shinsei Ryu, and Tadashi Takayanagi. Holographic entanglement entropy: an overview. *Journal of Physics A: Mathematical and Theoretical*, 42(50):504008, dec 2009.

[50] Mukund Rangamani and Tadashi Takayanagi. *Holographic Entanglement Entropy*, volume 931. Springer, 2017.

[51] Matthew Headrick. Lectures on entanglement entropy in field theory and holography. 7 2019.

[52] Leonard Susskind. Computational Complexity and Black Hole Horizons. *Fortsch. Phys.*, 64:24–43, 2016.

[53] Leonard Susskind and Ying Zhao. Switchbacks and the Bridge to Nowhere. 8 2014.

[54] Daniel A. Roberts, Douglas Stanford, and Leonard Susskind. Localized shocks. *JHEP*, 03:051, 2015.

[55] Douglas Stanford and Leonard Susskind. Complexity and Shock Wave Geometries. *Phys. Rev. D*, 90(12):126007, 2014.

[56] Leonard Susskind. Entanglement is not enough. *Fortsch. Phys.*, 64:49–71, 2016.

[57] Mohsen Alishahiha. Holographic Complexity. *Phys. Rev. D*, 92(12):126009, 2015.

[58] Adam R. Brown, Daniel A. Roberts, Leonard Susskind, Brian Swingle, and Ying Zhao. Holographic Complexity Equals Bulk Action? *Phys. Rev. Lett.*, 116(19):191301, 2016.

[59] Adam R. Brown, Daniel A. Roberts, Leonard Susskind, Brian Swingle, and Ying Zhao. Complexity, action, and black holes. *Phys. Rev. D*, 93(8):086006, 2016.

[60] Jose L.F. Barbon and Eliezer Rabinovici. Holographic complexity and spacetime singularities. *JHEP*, 01:084, 2016.

[61] Dean Carmi, Robert C. Myers, and Pratik Rath. Comments on Holographic Complexity. *JHEP*, 03:118, 2017.

[62] Ingo Peschel and Viktor Eisler. Exact results for the entanglement across defects in critical chains. *Journal of Physics A: Mathematical and Theoretical*, 45(15):155301, mar 2012.

[63] Constantin Bachas, Jan de Boer, Robbert Dijkgraaf, and Hirosi Ooguri. Permeable conformal walls and holography. *Journal of High Energy Physics*, 2002(06):027–027, jun 2002.

[64] N Andrei, A Bissi, M Buican, J Cardy, P Dorey, N Drukker, J Erdmenger, D Friedan, D Fursaev, A Konechny, C Kristjansen, I Makabe, Y Nakayama, A O'Bannon, R Parini, B Robinson, S Ryu, C Schmidt-Colinet, V Schomerus, C Schweigert, and G M T Watts. Boundary and defect CFT: open problems and applications. *Journal of Physics A: Mathematical and Theoretical*, 53(45):453002, oct 2020.

[65] Masaki Oshikawa and Ian Affleck. Defect lines in the ising model and boundary states on orbifolds. *Phys. Rev. Lett.*, 77:2604–2607, Sep 1996.

[66] Masaki Oshikawa and Ian Affleck. Boundary conformal field theory approach to the critical two-dimensional ising model with a defect line. *Nuclear Physics B*, 495:533–582, Jun 1997.

[67] Eugene Wong and Ian Affleck. Tunneling in quantum wires: A boundary conformal field theory approach. *Nuclear Physics B*, 417:403–438, Apr 1994.

[68] Claudio Chamon, Masaki Oshikawa, and Ian Affleck. Junctions of three quantum wires and the dissipative hofstadter model. *Phys. Rev. Lett.*, 91:206403, Nov 2003.

[69] Masaki Oshikawa, Claudio Chamon, and Ian Affleck. Junctions of three quantum wires. *Journal of Statistical Mechanics: Theory and Experiment*, 2006(02):P02008–P02008, feb 2006.

[70] Jun Kondo. Resistance minimum in dilute magnetic alloys. *Progress of Theoretical Physics*, 32(1):37–49, 07 1964.

[71] Ian Affleck. Conformal field theory approach to the kondo effect. *Acta Physica Polonica B*, 26(1):1869–1932, 1995.

[72] Andreas Karch and Lisa Randall. Locally localized gravity. *Journal of High Energy Physics*, 2001(05):008–008, may 2001.

[73] Andreas Karch and Lisa Randall. Open and closed string interpretation of SUSY CFT's on branes with boundaries. *Journal of High Energy Physics*, 2001(06):063–063, jun 2001.

[74] Oliver DeWolfe, Daniel Z. Freedman, and Hirosi Ooguri. Holography and defect conformal field theories. *Phys. Rev. D*, 66:025009, Jul 2002.

[75] Shira Chapman, Dongsheng Ge, and Giuseppe Policastro. Holographic Complexity for Defects Distinguishes Action from Volume. *JHEP*, 05:049, 2019.

[76] John von Neumann. Mathematische grundlagen der quantenmechanik. 1932.

[77] Alfred Wehrl. General properties of entropy. *Rev. Mod. Phys.*, 50:221–260, Apr 1978.

[78] Curtis G. Callan, Jr. and Frank Wilczek. On geometric entropy. *Phys. Lett. B*, 333:55–61, 1994.

[79] Christoph Holzhey, Finn Larsen, and Frank Wilczek. Geometric and renormalized entropy in conformal field theory. *Nucl. Phys. B*, 424:443–467, 1994.

[80] Pasquale Calabrese and John L. Cardy. Entanglement entropy and quantum field theory. *J. Stat. Mech.*, 0406:P06002, 2004.

[81] Pasquale Calabrese and John Cardy. Entanglement entropy and conformal field theory. *J. Phys. A*, 42:504005, 2009.

[82] Ian Affleck, Nicolas Laflorencie, and Erik S Sørensen. Entanglement entropy in quantum impurity systems and systems with boundaries. *Journal of Physics A: Mathematical and Theoretical*, 42(50):504009, dec 2009.

[83] Kazuhiro Sakai and Yuji Satoh. Entanglement through conformal interfaces. *Journal of High Energy Physics*, 2008(12):001–001, dec 2008.

[84] Leonard Susskind. Three lectures on complexity and black holes. 2020.

[85] Dean Carmi, Shira Chapman, Hugo Marrochio, Robert C. Myers, and Sotaro Sugishita. On the Time Dependence of Holographic Complexity. *JHEP*, 11:188, 2017.

[86] Shira Chapman, Hugo Marrochio, and Robert C. Myers. Holographic complexity in Vaidya spacetimes. Part I. *JHEP*, 06:046, 2018.

[87] Shira Chapman, Hugo Marrochio, and Robert C. Myers. Holographic complexity in Vaidya spacetimes. Part II. *JHEP*, 06:114, 2018.

[88] Luis Lehner, Robert C. Myers, Eric Poisson, and Rafael D. Sorkin. Gravitational action with null boundaries. *Phys. Rev. D*, 94:084046, Oct 2016.

[89] Erhard Schmidt. Zur theorie der linearen und nichtlinearen integralgleichungen. *Mathematische Annalen*, 63:433–476, Dec 1907.

[90] Arthur Ekert. Entangled quantum systems and the schmidt decomposition. *American Journal of Physics*, 63:415, 1995.

[91] Asher Peres. Higher order schmidt decompositions. *Physics Letter A*, 202:16–17, Jun 1995.

[92] M. Nielsen and I. Chuang. *Quantum Computation and Quantum Information*. Cambridge University Press, 2000.

[93] Elliott H. Lieb and Mary Beth Ruskai. A fundamental property of quantum-mechanical entropy. *Phys. Rev. Lett.*, 30:434–436, Mar 1973.

[94] Elliot H. Lieb. Proof of the strong subadditivity of quantum-mechanical entropy. *Journal of Mathematical Physics*, 14, Nov 1973.

[95] Elliott H. Lieb and Mary Beth Ruskai. Entropy inequalities. *Communications in Mathematical Physics*, 18:160–170, Jun 1970.

[96] V. Vedral. The role of relative entropy in quantum information theory. *Rev. Mod. Phys.*, 74:197–234, Mar 2002.

[97] J. Williamson. On the Algebraic Problem Concerning the Normal Forms of Linear Dynamical Systems. *American Journal of Mathematics*, 58(1):141–163, 1936.

[98] R. Simon, E. Sudarshan, and N. Mukunda. Gaussian-Wigner distributions in quantum mechanics and optics. *Phys. Rev. A*, 36:3868–3880, 1987.

[99] Tommaso F Demarie. Pedagogical introduction to the entropy of entanglement for gaussian states. *European Journal of Physics*, 39(3):035302, mar 2018.

[100] J. Eisert, M. Cramer, and M. B. Plenio. Colloquium: Area laws for the entanglement entropy. *Rev. Mod. Phys.*, 82:277–306, Feb 2010.

[101] Tatsuo Azeyanagi, Tadashi Takayanagi, Andreas Karch, and Ethan G Thompson. Holographic calculation of boundary entropy. *Journal of High Energy Physics*, 2008(03):054–054, mar 2008.

[102] J.David Brown and Marc Henneaux. Central charges in the canonical realization of asymptotic symmetries: an example from three-dimensional gravity. *Communications in Mathematical Physics*, 104(2):207–226, jun 1986.

[103] Alice Bernamonti, Federico Galli, Juan Hernandez, Robert C. Myers, Shan-Ming Ruan, and Joan Simon. Aspects of The First Law of Complexity. *J. Phys. A*, 53:294002, 2020.

[104] Alice Bernamonti, Federico Galli, Juan Hernandez, Robert C. Myers, Shan-Ming Ruan, and Joan Simón. First Law of Holographic Complexity. *Phys. Rev. Lett.*, 123(8):081601, 2019.

[105] Tadashi Takayanagi. Holographic Dual of BCFT. *Phys. Rev. Lett.*, 107:101602, 2011.

[106] Mitsutoshi Fujita, Tadashi Takayanagi, and Erik Tonni. Aspects of AdS/BCFT. *JHEP*, 11:043, 2011.

[107] Pasquale Calabrese, John Cardy, and Erik Tonni. Entanglement negativity in extended systems: A field theoretical approach. *J. Stat. Mech.*, 1302:P02008, 2013.